Supporting Information for:

A Million-fold Increase in C-H Bond Acidity Gives Palladium a Key Advantage in C(sp^3)-H Activation Compared to Nickel

Lirong Lin,[a] *Tim K. Schramm,*[b] *Pavel Kucheryavy,*[a] *Roger A. Lalancette,*[a] *Andreas Hansen,*[b*] *and Demyan E. Prokopchuk*[a*]

[a]Department of Chemistry, Rutgers University-Newark, Newark, New Jersey 07102, United States. *demyan.prokopchuk@rutgers.edu

[b]Mulliken Center for Theoretical Chemistry, Clausius-Institut für Physikalische und Theoretische Chemie, Rheinische Friedrich-Wilhelms Universität Bonn, Bonn 53115, Germany. *hansen@thch.uni-bonn.de

Part A

Experimental

Contents

General Comments

All reactions were carried out under an atmosphere of nitrogen using standard glove box or high vacuum line (Schlenk) techniques unless stated otherwise. All reagents and solvents were stored under inert gas unless stated otherwise. Inert atmosphere reactions and workup protocols used HPLC-grade, inhibitor-free solvents were dried and degassed over activated alumina using an IT/Inert solvent purification system. Additionally, 1,4-dioxane, *n*-pentane, tetrahydrofuran (THF), fluorobenzene (PhF), diethyl ether (Et_2O), toluene, acetonitrile (MeCN), 1,2-dichloroethane (DCE) and dichloromethane (DCM) were dried over 10% w/v activated 3 Å molecular sieves.[1] Deuterated solvents were subjected to three freeze-pump-thaw cycles and dried over 10% w/v activated 3 Å molecular sieves in a glove box. Glassware was dried overnight at 140 °C and cooled under dynamic vacuum in a glove box antechamber. Celite and glass fiber filter circles (1.6 μm) were dried in an oven at 140 °C overnight prior to use in the glove box. Column chromatography was performed using silica gel (60 Å porosity, 40-63 μm particle size). Elemental analyses were run by CENTC Elemental Analysis Facility (Department of Chemistry, University of Rochester) on a PerkinElmer 2400 Series II Analyzer. Compounds **PCH_2P**[2, 3] and $[H(OEt_2)_2][B(C_6F_5)_4]$[4] (DCl ($Et_2O$) instead of HCl ($Et_2O$) was used for $[D(OEt_2)_2][B(C_6F_5)_4]$) were prepared using known literature procedures while the known complex **[PdBr]**[3] was isolated using a modified workup protocol as described later. $[^nBu_4N][B(C_6F_5)_4]$ was prepared using a known procedure[5] but using $KB(C_6F_5)_4$ as the anion source and recrystallizing via vapor diffusion from fluorobenzene/pentane. To minimize cross-contamination with ethereal solvent vapors inside the glove box for all acid-base reactions, solvents were stored in Teflon-sealed Schlenk vessels when not in use.

NMR Spectroscopy. Experiments were conducted on Bruker Avance III HD 500 MHz NMR and Varian Inova 600 MHz NMR spectrometers. Spectra for ^1H and ^{13}C were referenced to their respective residual protio solvent signal,[6] ^{31}P to external 85% H_3PO_4 (0 ppm), ^{19}F to external $C_6H_5CF_3$ (-63.72 ppm). NMR signal assignments were made by routine one- and two-dimensional experiments provided by Bruker and Varian, including ^1H-^1H COSY, ^1H-^1H NOESY, ^1H-^{13}C HSQC, ^1H-^{13}C HMBC, ^1H-^{31}P HMBC (optimized for $^1J(PH) = 200$ Hz, long range $J(PH) = 8$ Hz). All NMR measurements were carried out at 25 ºC unless otherwise stated. For Van't Hoff Analyses from VT-NMR data, S/N (Signal to Noise) ratios were calculated for each signal in Topspin by using the "SINo" function. The relative error for peak integrals is 1/(S/N). For VT-NMR experiments, the probe temperature was calibrated using Sigma-Aldrich methanol-d4 NMR reference standard.

DOSY NMR experiments for constructing external calibration curves (ECCs) were conducted on Bruker Avance III HD 500 MHz spectrometer using the dstebpgp3s pulse program with 5 s relaxation delay (d1), and 0.1 s diffusion delay (d20). Duration of the gradient delay (p30) was optimized for each individual compound in the range between 500 and 900 μs using the dstebpgp3s1d pulse program. For the equilibrium measuements, p30 was set to 900 μs. Data was processed in Mnova 15.1, GNAT,[7] and OriginPro software. For the ECC, each molecule was dissolved on CH_2Cl_2 with a concentration of 1 mg/mL. Low analyte concentrations were required to minimize ion pairing in solution. For equilibrium K_2, two independently prepared samples were used to measure diffusion coefficients. Sample 1 contained 1.0 mg **[PdBr]** and 1.1 mg **$[H_3NAr^F][B(C_6F_5)_4]$** dissolved in 1 mL CD_2Cl_2 and Sample 2 contained 7.4 mg **[PdBr]** and 8.1 mg **$[H_3NAr^F][B(C_6F_5)_4]$** dissolved in 0.6 mL CD_2Cl_2.

Variable temperature ^{31}P NMR experiments with inverse gated decoupling were performed on a 500 MHz Avance III HD NMR spectrometer in the range between -40 and 70 °C in PhF and between -70

and 25 °C in CD_2Cl_2. Spectra were collected in 10 °C intervals. NMR spectra were fitted by trial and error using the DNMR (dynamic NMR)[8] package in Topspin. The exchange rate constant for each modeled line broadening was used to generate an Eyring plot, providing thermodynamic information about the rotation barrier about the Pd-Br-Pd axis in **[Pd-Br-Pd]$^+$**.

Error Propagation for Acid-Base Reactions. For VT-NMR equilibrium experiments, the S/N for all integrals was determined using the "SINo" function as described above. Sample masses were weighed using an analytical balance inside a glove box with a readability of 0.1 mg and error of ± 0.1 mg for each recorded mass. Solvent volumes for NMR samples were measured using standard 1 mL syringes (HSW Norm-Ject) with an estimated error of ± 0.02 mL. For equilibrium measurements and thermochemical calculations, standard error propagation equations were applied to all equations. In many cases, the largest contributor to the error at elevated temperatures in ^{31}P spectra was for **[Pd-Br-Pd]$^+$**, which shows broad signals, resulting in low S/N (Signal to Noise) ratios. For ^{1}H-^{1}H EXSY NMR experiments, noise was integrated to match the size of the peak with the largest dimension. S/N ratios were calculated for each signal for the error calculations.

X-Ray Crystallography. Single crystals of **[PdBr]**, **[Pd-Br-Pd]$^+$**, **[PdCH$_2$]$^+$** and **[H$_3$NAr^{Cl}][B(C$_6$F$_5$)$_4$]** were selected and mounted using Paratone onto a nylon fiber and cooled to the data collection temperature of 100(2) K with a stream of dry nitrogen gas. X-ray diffraction intensities were collected on a Bruker SMART APEX II CCD Diffractometer using CuKα (1.54178 Å) radiation. For all structures, the CheckCIF routine and structure factor analyses were performed by Platon[9] via https://checkcif.iucr.org/. Graphics were generated using Mercury. All crystallographic data has been deposited with the Cambridge Crystallographic Data Center and is available free of charge through the CCDC online database (https://www.ccdc.cam.ac.uk/).

Electrochemistry. Cyclic voltammetry experiments were conducted under N_2 at 295 ± 3 K using a standard three-electrode setup consisting of a 1 mm PEEK-encased glassy carbon working electrode (eDAQ), graphite rod counter electrode, and Ag wire pseudoreference electrode. The working electrode was polished with 0.25 μm diamond polishing paste, lapping oil, and a rayon microcloth pad (Buehler) inside a glove box and thoroughly rinsed with the solvent used in the corresponding experiment. A Gamry Reference 620 potentiostat, Gamry 1010 potentiostat and Gamry software were used for data collection and analysis. Unless stated otherwise, samples contained 0.2 M [^{n}Bu$_4$N][B(C$_6$F$_5$)$_4$], organic solvent (1.5 mL), and 1 mM analyte. The uncompensated solution resistance (R_u) was measured for each electrochemical solution and post-*iR* correction (positive feedback) was applied to all CV traces. All CVs are referenced to the $Fc^{+/0}$ redox couple (0 V).

Syntheses

[PdBr]

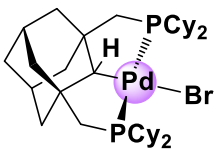

This known complex[3] was purified using a modified protocol. In the glovebox, $PdBr_2$(COD) (374 mg, 1.0 equiv., 1.0 mmol) and K_3PO_4 (254 mg, 1.2 equiv., 1.2 mmol) were suspended in 100 mL dioxane in

a thick-walled glass pressure tube followed by the addition of the known 1,3-bis(dicyclohexylmethylphosphino) adamantane ligand **PCH_2P** (612 mg, 1.1 equiv., 1.1 mmol). The tube was sealed and heated at 100 ºC in the fume hood for three hours. Then, the reaction vessel was cooled to room temperature and brought into the glovebox. Next, 100 mL Et_2O was added to the mixture and the solution was filtered through a 60 mL medium-pore glass frit equipped with a pad of Celite. The filtrate was dried and extracted with a mixture of Et_2O:pentane (1:1, 30 mL x 2) to obtain an orange liquid, which was tested by TLC (thin layer chromatography) using 5:1 hexane:Et_2O as the mobile phase under air (Fig. S1, left). Column chromatography was conducted under air with a glass column ($\varnothing = 2$ cm) with a medium-pore glass frit and packed with approximately 17 cm of silica. The column was flushed using a gradient elution of hexane:Et_2O (15:1; 9:1; 5:1; 1:1, 100 mL for each solvent mixture). The product began eluting from the column after collecting approximately 150 mL of yellow liquid, which was indicated by TLC (hexane: Et_2O = 5:1) (Fig. S1, middle). After drying the nearly pure fraction, the yellow solid (180 mg, 24%) was suspended and stirred in 1.0 mL Et_2O for two hours. The analytically pure pale-yellow product (Fig. S1, right) was obtained by isolation on a medium-pore glass frit and the solid was then dried under high vacuum overnight at 80 °C before taking into the glove box (126 mg, 17%). X-ray-quality crystals of **[PdBr]** were obtained by a concentrated pentane or $CHCl_3$ solution at room temperature and NMR matches previously reported spectral data[3]. Attempts to improve the yield by changing the starting Pd source, reaction solvent, or base were unsuccessful.

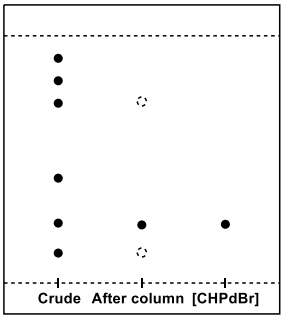

Figure S1- TLC (Hexane: Et_2O = 5:1) of the crude product before column chromatography (left), after column chromatography (middle), and the analytically pure product **[PdBr]** after washing with Et_2O (right).

$[Pd\text{-}Br\text{-}Pd]^+$

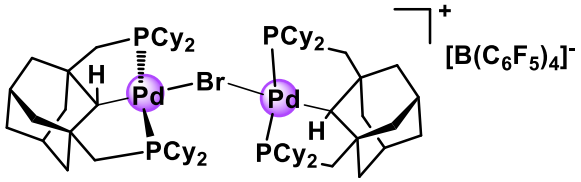

In the glovebox, **[PdBr]** (44.4 mg, 0.060 mmol) and $K[B(C_6F_5)_4]$ (21.6 mg, 0.030 mmol) were added in a 20 ml vial followed by 3.0 mL DCM. The reaction turned light orange immediately. After stirring overnight at room temperature, the reaction mixture was pipetted through a glass fiber filter plug to remove the white precipitate and obtain an orange filtrate. The crude product was evaporated to dryness and rinsed with pentane (2.0 mL x 3). Then, 2.0 mL Et_2O was added and the solution was stirred for 10 min. The pale-yellow solid was isolated on a medium-pore glass frit and washed with Et_2O (2.0 mL), washing away a brown impurity. The resulting pale-yellow product (50 mg, 80%) was obtained after drying under high vacuum. Anal. calcd (%) for $C_{96}H_{122}Pd_2P_4BBrF_{20}$: C 55.34, H 5.90, N 0.00; found: C 54.87, H 5.70, N 0.03.

^{1}H NMR (500 MHz, CD_2Cl_2, 25 ºC): δ 3.28 (s, br, 2H, C*H*Pd), 2.28-0.94 (120H). $^{31}P\{^{1}H\}$ NMR (202 MHz, CD_2Cl_2, 25 ºC): δ 55.0 (br), 50.8 (br) ppm. $^{31}P\{^{1}H\}$ NMR (202 MHz, CD_2Cl_2, -60 ºC): δ 56.0 (d, $^{1}J_{PP}$ = 318.59 Hz), 48.8 (d, $^{1}J_{PP}$ = 318.58 Hz) ppm. ^{13}C NMR (151 MHz, CD_2Cl_2, 25 ºC) δ 149.51 ($B(C_6F_5)_4$), 147.95 ($B(C_6F_5)_4$), 139.63 ($B(C_6F_5)_4$), 137.69 ($B(C_6F_5)_4$), 136.06 ($B(C_6F_5)_4$), 124.67 (br, $B(C_6F_5)_4$), 80.34 (*C*H-Pd), 47.49, 46.10, 44.49, 36.43, 35.77, 31.35, 30.38, 29.62, 28.08, 27.56, 27.36, 26.73, 26.55 ppm.

Protonation of [PdBr] with $H(Et_2O)_2[B(C_6F_5)_4]$

In the glovebox, **[PdBr]** (14.8 mg, 0.020 mmol) was dissolved in 1.0 ml PhF in a Schlenk flask, sealed, then connected to a Schlenk line and cooled to -40 ºC. Next, $[H(OEt_2)_2][B(C_6F_5)_4]$ (16.6 mg, 0.020 mmol) dissolved in 1.0 mL PhF was added to the solution dropwise. After addition, the solution turned yellow and was stirred at -40 ºC for 2 min. The cold bath was removed and the reaction was stirred at room temperature for 20 mins. The color of the solution turned orange while warming to room temperature due to a change in concentration from primarily yellow **[Pd-Br-Pd]**$^{+}$ at lower temperature and increasing concentrations of orange **[PdCH$_2$]**$^{+}$ at room temperature (Fig S2). The solvent was removed under a high vacuum for three hours. X-ray-quality crystals containing a mixture of orange **[PdCH$_2$]**$^{+}$ and pale yellow **[Pd-Br-Pd]**$^{+}$ were obtained by layering a concentrated toluene solution with pentane at room temperature. Suitable crystals were hand-picked from these batches. From batch to batch, **[Pd-Br-Pd]**$^{+}$ crystallized as pale yellow needles, pale yellow rods, or pale yellow plates. Crystallization via toluene/Et_2O vapor diffusion at room temperature solely produced colorless crystals of **[Pd-Br-Pd]**$^{+}$, as excess Et_2O drives the reaction equilibrium towards formation of **[Pd-Br-Pd]**$^{+}$ in solution.

^{1}H NMR (500 MHz, CD_2Cl_2, 25 ºC): δ 16.31 (s, br, **[HBrH•2OEt$_2$]**$^{+}$), 4.18 (CH_2, Et_2O), 3.97 (CH_2, Et_2O), 3.30 (br, C*H*-Pd, **[Pd-Br-Pd]**$^{+}$), 2.27 (CH_{Ad}), 2.24 - 1.10 ppm (mixture of Et_2O, Ad, Cy resonances from **[PdCH$_2$]**$^{+}$ and **[Pd-Br-Pd]**$^{+}$. Some Cy and Ad resonances were identified via 2D NMR spectral analysis: 2.17 (CH_{Cy}-P), 2.05 (CH_2-P), 1.69 and 1.93 (CH_{2Ad}) ppm), 0.49 (br, 2H, CH_2-Pd, **[PdCH$_2$]**$^{+}$) ppm. $^{31}P\{^{1}H\}$ NMR (202 MHz, CD_2Cl_2, 25 ºC): δ 66.4 (s, **[PdCH$_2$]**$^{+}$), 55.2 (br, **[Pd-Br-Pd]**$^{+}$), 50.8 (br, **[Pd-Br-Pd]**$^{+}$) ppm. $^{31}P\{^{1}H\}$ NMR (202 MHz, CD_2Cl_2, -60 ºC): δ 67.0 (s, **[PdCH$_2$]**$^{+}$), 55.9 (d, $^{2}J_{PP}$ = 318.52 Hz, **[Pd-Br-Pd]**$^{+}$), 48.7 (d, $^{2}J_{PP}$ = 318.48 Hz, **[Pd-Br-Pd]**$^{+}$) ppm. ^{13}C NMR (126 MHz, CD_2Cl_2, 25 ºC) δ 163.29 (m, $^{1}J_{CF}$ = 244.8 Hz, ($B(C_6F_5)_4$), 148.59 (m, $^{1}J_{CF}$ = 241.6 Hz, $B(C_6F_5)_4$), 137.71 (m, $^{1}J_{CF}$ = 243.6 Hz, $B(C_6F_5)_4$), 124.52 (br, $B(C_6F_5)_4$), 69.98 (OCH_2), 58.51(t, *J* = 11.4 Hz, CH_2-Pd of **[PdCH$_2$]**$^{+}$), 46.00, 44.81 (t, *J* = 3.0 Hz, quaternary C_{Ad}), 43.24 (s, CH_{2Ad}), 42.36 (t, *J* = 7.5 Hz, PCH_2), 36.27, 35.56 (t, *J* = 11.0 Hz, PCH_{Cy}), 34.31, 31.24, 30.12, 29.90 (s, CH_{Ad}), 29.59, 29.45, 28.83, 27.97, 27.43, 27.21, 27.07, 26.93, 26.59, 26.41, 25.94, 14.20 (s, OCH_2CH_3).

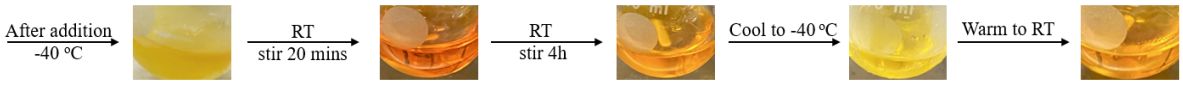

Figure S2- Color change upon addition of $[H(OEt_2)_2][B(C_6F_5)_4]$ to **[PdBr]** and the temperature-dependent color changes after protonation.

$[H_3NAr^{Cl}][B(C_6F_5)_4]$

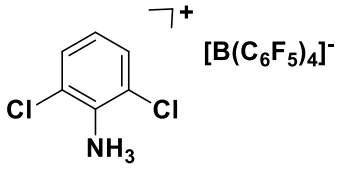

In the glovebox, 2,6-dichlroaniline (32.4 mg, 0.20 mmol) and $K[B(C_6F_5)_4]$ (143.6 mg, 0.20 mmol) were suspended in 10 ml DCM in a Schlenk flask, sealed, then connected to a schlenk line. While stirring under N_2, the reaction was bubbled with $HCl_{(g)}$ for 10 min using a PEEK tube pierced through a rubber septum (Fig. S3). The tube was then removed, and the reaction was stirred under N_2 for 10 min. The solvent was then removed under high vacuum to obtain a white solid and the schlenk flask was taken into a glove box. The analytically pure white product was extracted with DCM (10 mL), filtered through a glass fiber filter plug and dried under high vacuum (122 mg, 73%). X-ray-quality crystals of **$[H_3NAr^{Cl}][B(C_6F_5)_4]$** were obtained by crystallization via Toluene/pentane vapor diffusion at room temperature. Anal. calcd (%) for $C_{30}H_6NCl_2BF_{20}$: C 42.79, H 0.72, N 1.66; found: C 43.02, H 1.01, N 1.79.

^{1}H NMR (500 MHz, CD_2Cl_2): δ 7.58 (d, 2H, *m*-C*H*), 7.51 (t, 1H, *p*-C*H*), 7.09 (3H, NH_3) ppm. ^{19}F NMR (471 MHz, CD_2Cl_2, 25 °C): δ -133.23, -163.07 (t), -167.08 ppm.

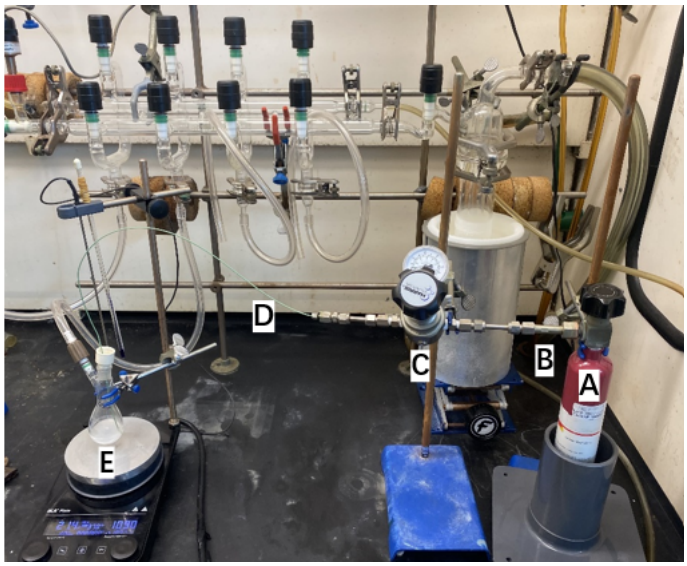

Figure S3- The $HCl_{(g)}$ addition setup. A lecture bottle containing $HCl_{(g)}$ (A) is connected via stainless steel compression fittings (B) to a corrosion resistant single-stage gas regulator (C; Harris HP743 Series, Model 743-050-000-C). The outlet on the low-pressure side contains polyether ether ketone (PEEK) tubing (D; 0.03" ID, 1/16" OD) attached via compression fitting to the stainless-steel outlet tube. The PEEK tubing is pierced directly into a pre-formed hole in a rubber septum connected to a Schlenk flask (E) under N_2.

$[H_3NAr^F][B(C_6F_5)_4]$

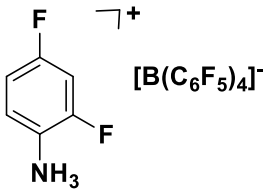

In the glovebox, 2,6-difluoroaniline (20 μL, 0.20 mmol) and $K[B(C_6F_5)_4]$ (144 mg, 0.20 mmol) were suspended in 10 ml DCM in a schlenk flask, sealed, then connected to a schlenk line. While stirring under N_2, the reaction was bubbled with HCl gas for 5 min (Fig. S3). The tube was then removed, and then the reaction was stirred under N_2 for 10 min. The solvent was then removed under high vacuum to obtain a white solid and the schlenk flask was taken into a glove box. The analytically pure white product was extracted with DCM (10 mL), filtered through a medium-pore glass frit and dried under high vacuum (94 mg, 58%). Anal. calcd (%) for $C_{30}H_6F_{22}BN$: C 44.53, H 0.75, N 1.73; found: C 44.926, H 1.373, N 2.138.

^{1}H NMR (500 MHz, CD_2Cl_2): δ 8.52 (s, 3H, N*H*$_3$), 7.55 (m 1H), 7.16 (m, 1H), 7.10 (m, 1H) ppm. ^{19}F NMR (471 MHz, CD_2Cl_2, 25 °C): δ -102.38, -119.96, -133.24, -162.94, -167.03.

VT-NMR and Kinetic Analysis of $[Pd\text{-}Br\text{-}Pd]^+$

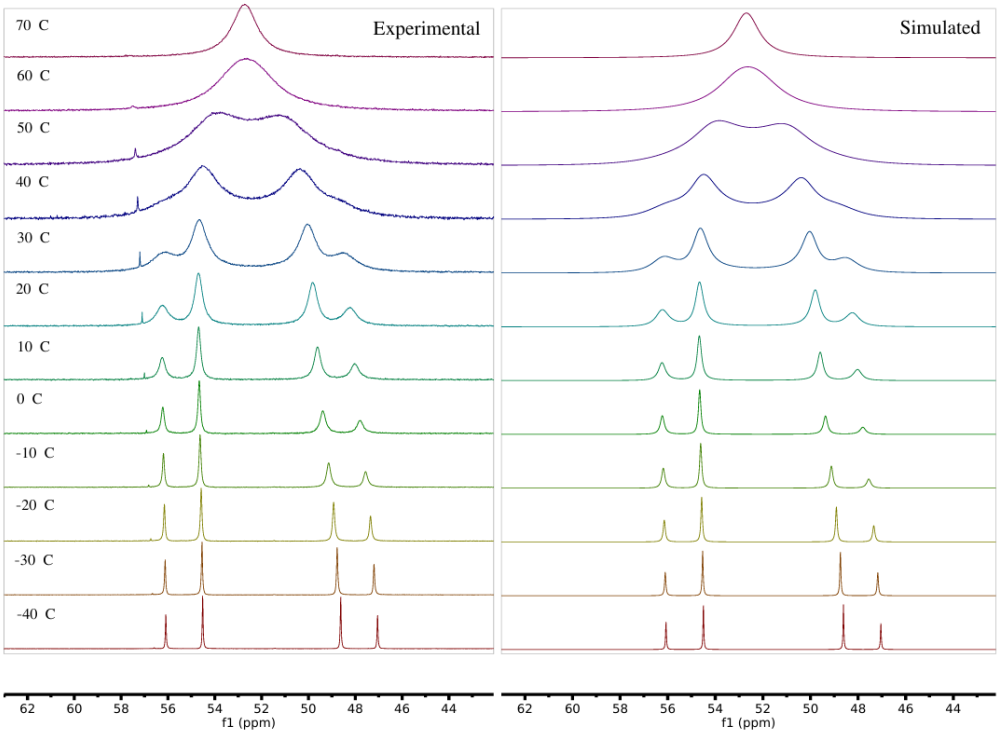

Figure S4- Experimental (left) and simulated (right) VT ^{31}P NMR spectrum of **$[Pd\text{-}Br\text{-}Pd]^+$** (202 MHz, PhF).

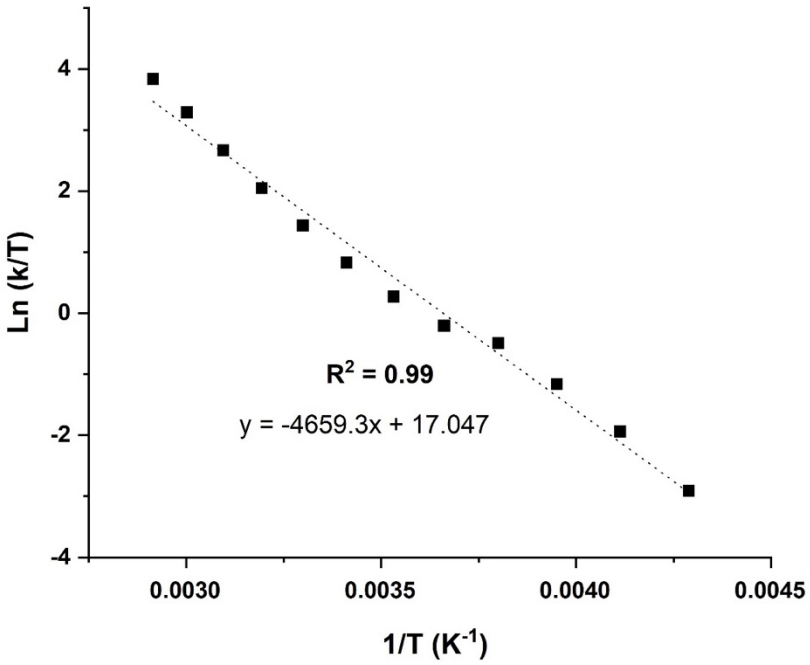

Figure S5- Eyring Plot for **[Pd-Br-Pd]**$^+$ in PhF, where $\Delta H^{\ddagger}$ = 9.3 ± 0.3 kcal/mol, $\Delta S^{\ddagger}$ = -13.4 ± 0.5 cal/(mol·K), and $\Delta G^{\ddagger}_{298K}$ = 13.3 ± 0.3 kcal/mol.

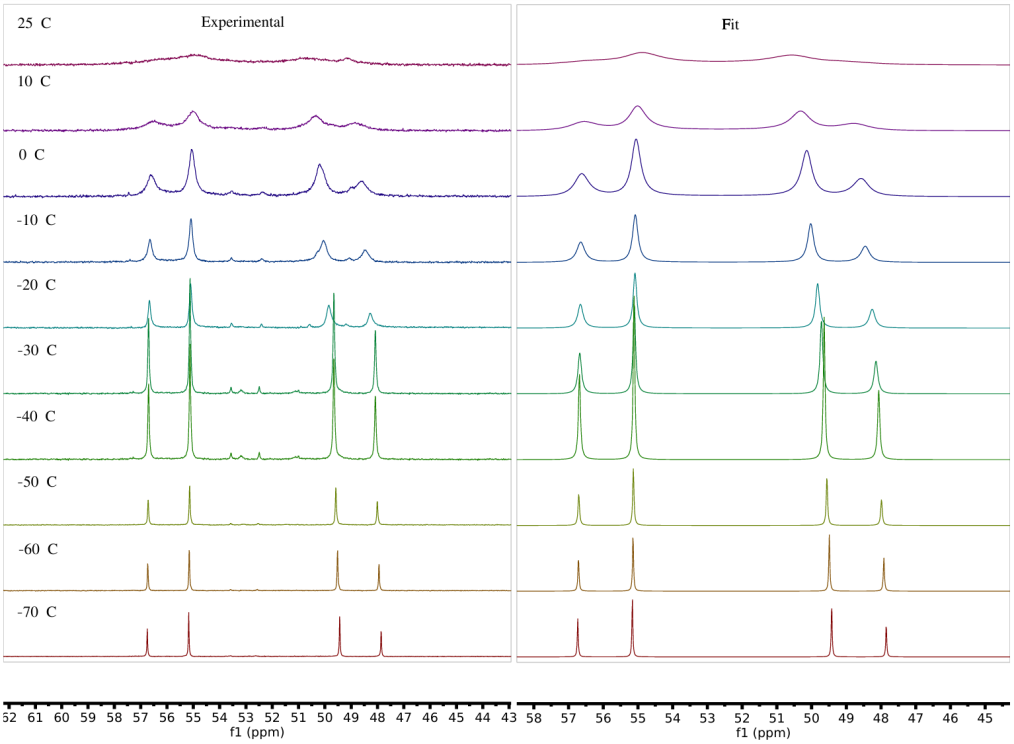

Figure S6- Experimental (left) and simulated (right) VT ^{31}P NMR spectrum of **[Pd-Br-Pd]**$^+$ (202 MHz, CD_2Cl_2).

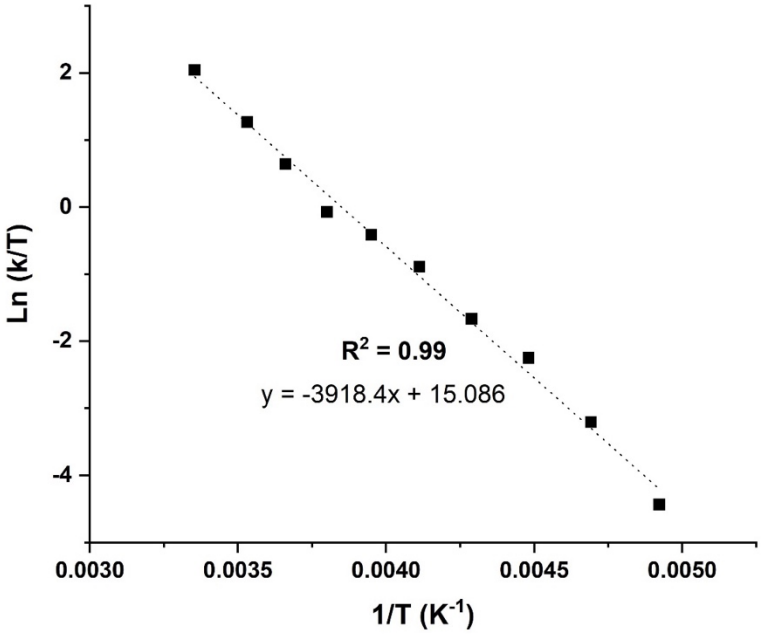

Figure S7- Eyring Plot for **[Pd-Br-Pd]**$^+$ in CD_2Cl_2, where $\Delta H^{\ddagger} = 7.8 \pm 0.2$ kcal/mol, $\Delta S^{\ddagger} = -17.3 \pm 0.9$ cal/(mol·K), and $\Delta G^{\ddagger}_{298K} = 13.0 \pm 0.4$ kcal/mol.

Acid-Base Reactions

$[H(OEt_2)_2][B(C_6F_5)_4]$

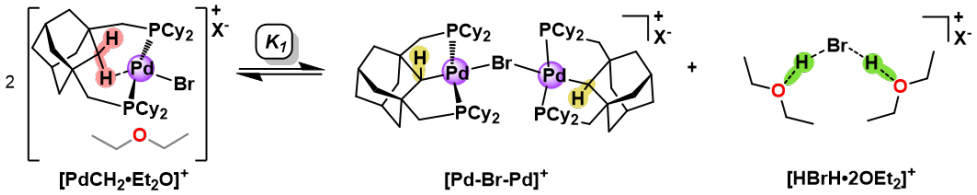

Scheme S1- Proposed equilibrium processed upon addition of $[H(OEt_2)_2][B(C_6F_5)_4]$ to **[PdBr]**. $X^- = B(C_6F_5)_4^-$.

Van't Hoff analysis

In the glovebox, **[PdBr]** (14.8 mg, 0.020 mmol) was dissolved in 1.0 ml PhF in a Schlenk flask, sealed, then connected to a Schlenk line and cooled to -40 ºC. Next, $[H(OEt_2)_2][B(C_6F_5)_4]$ (16.6 mg, 0.020 mmol) in 1.0 mL PhF was added to the solution dropwise. After addition, the solution was stirred at -40 ºC for 2 min. The cold bath was removed, and the reaction was stirred at room temperature for 20 min. The color of the solution turned into orange while warming to room temperature. The solvent was removed under high vacuum for 3 h. The residue was dissolved in CD_2Cl_2 (0.55 mL), which gives the initial concentration c_i as 36 ± 3.7% mmol/L. Then, $^{31}P\{^1H\}$ NMR spectra were collected from -70 ºC to 25 ºC in 10 ºC intervals (Fig. S10). The concentration of **[PdCH₂•Et₂O]**$^+$ (c(PdCH$_2$)) and **[Pd-Br-Pd]**$^+$ (c(Pd-Br-Pd)) were calculated using equation S1 and S2 with integrals I(PdCH$_2$) and I(Pd-Br-Pd). The equilibrium constant K_1 was calculated at all temperatures using equation S3, assuming that the concentration of **[Pd-Br-Pd]**$^+$ is equal to the concentration of **[HBrH•2OEt₂]**$^+$. With the data in Table

S1, Van't Hoff plots were generated (Fig. S8-9, blue), allowing the calculation of the thermochemical values for the equilibrium (Table S2). An identical deuteration experiment was conducted with $[D(OEt_2)_2][B(C_6F_5)_4]$ (16.6 mg, 0.020 mmol) (Fig. S11) and the corresponding thermochemical values were calculated (Table S1-2) with Van't Hoff analysis (Fig. S8-9, red).

$$c(PdCH_2) = \frac{I(PdCH_2)}{0.5\ I(\text{Pd-Br-Pd}) + I(PdCH_2)} \times c_i \quad \text{(S1)}$$

$$c(\text{Pd-Br-Pd}) = \frac{0.5\ I(\text{Pd-Br-Pd})}{0.5\ I\ (\text{Pd-Br-Pd}) + I(PdCH_2)} \times c_i \quad \text{(S2)}$$

$$K_1 = \frac{c(\text{Pd-Br-Pd})^2}{c(PdCH_2)^2} \quad \text{(S3)}$$

Table S1- VT-NMR peak integration and K_1 data for **$[PdCH_2{\bullet}Et_2O]^+$** and **$[Pd\text{-}Br\text{-}Pd]^+$** reacting with $[H(OEt_2)_2][B(C_6F_5)_4]$ or $[D(OEt_2)_2][B(C_6F_5)_4]$. Integrals are measured relative to the ^{31}P resonance for **$[PdCH_2{\bullet}Et_2O]^+$** which is set to exactly 1.

		H^+			D^+		
T(°C)	***I*(PdCH₂)**	***I*(Pd-Br-Pd)**	***K*₁**	**Ln *K*₁**	***I*(Pd-Br-Pd)**	***K*₁**	**Ln *K*₁**
25	1.00	1.38 (15)	0.48 (13)	-0.74 (28)	1.29 (14)	0.42 (11)	-0.88 (28)
10	1.00	1.79 (10)	0.80 (13)	-0.22 (16)	1.52 (7)	0.58 (8)	-0.55 (14)
0	1.00	1.87 (4)	0.87 (8)	-0.13 (9)	1.67 (4)	0.70 (7)	-0.36 (10)
-10	1.00	1.99 (7)	0.99 (11)	-0.01 (11)	1.78 (3)	0.79 (7)	-0.23 (9)
-20	1.00	2.09 (9)	1.09 (14)	0.09 (13)	1.89 (6)	0.89 (10)	-0.11 (8)
-30	1.00	2.20 (3)	1.21 (10)	0.19 (8)	1.92 (3)	0.92 (8)	-0.08 (8)
-40	1.00	2.31 (2)	1.33 (10)	0.20 (8)	1.97 (3)	0.97 (8)	-0.03 (8)
-50	1.00	2.36 (3)	1.39 (11)	0.33 (8)	1.96 (3)	0.96 (8)	-0.04 (8)
-60	1.00	2.29 (3)	1.31 (10)	0.27 (8)	1.98 (3)	0.98 (8)	-0.02 (8)
-70	1.00	2.26 (2)	1.28 (10)	0.24 (8)	1.95 (3)	0.95 (8)	-0.05 (8)

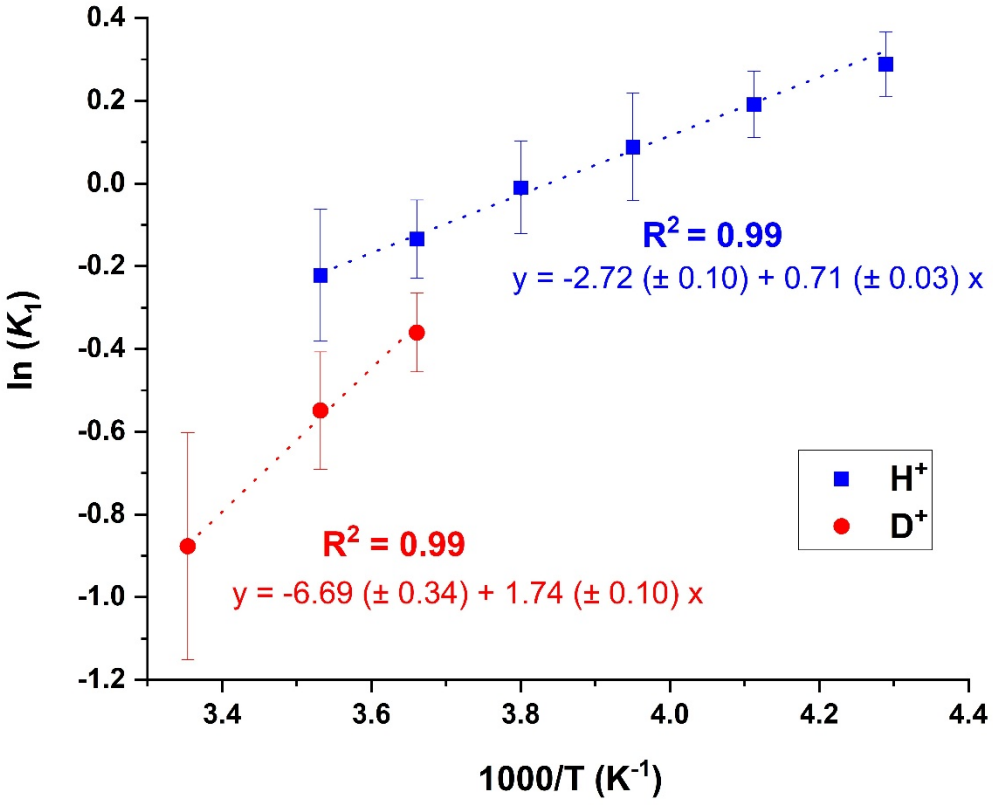

Figure S8- Linear region of Van't Hoff plot for the reaction with $[H(OEt_2)_2][B(C_6F_5)_4]$.

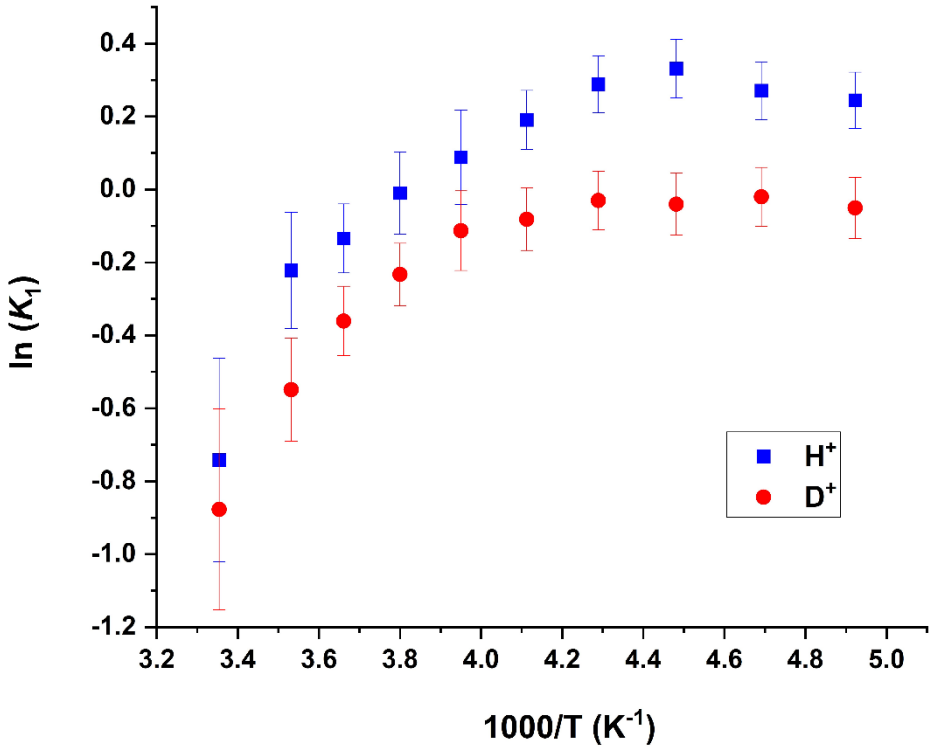

Figure S9- Full temperature profile of Van't Hoff plot for the reaction with $[H(OEt_2)_2][B(C_6F_5)_4]$ (blue) and $[D(OEt_2)_2][B(C_6F_5)_4]$ (red) in CD_2Cl_2.

Table S2- Thermochemical data values for the equilibrium upon reaction with $[H(OEt_2)_2][B(C_6F_5)_4]$ and $[D(OEt_2)_2][B(C_6F_5)_4]$ in CD_2Cl_2.

	ΔH (kcal/mol)	ΔS (cal/(mol·K))	ΔG_{298K} (kcal/mol)
H^+	-1.42 ± 0.05	-5.44 ± 0.20	0.20 ± 0.08
D^+	-3.47 ± 0.20	-13.39 ± 0.69	0.52 ± 0.29

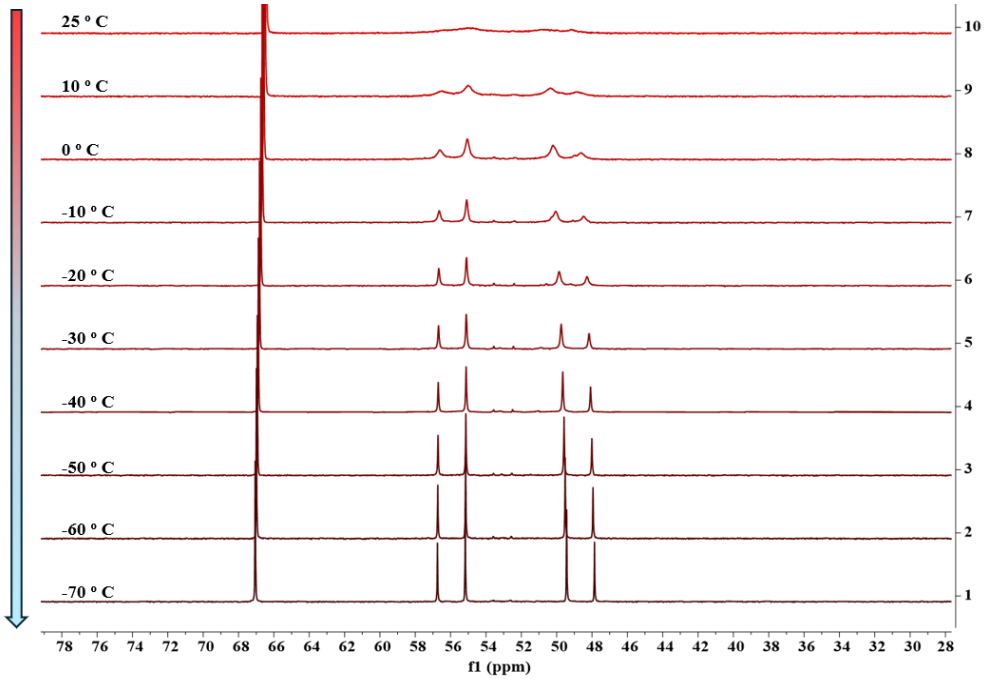

Figure S10- Variable temperature inverse-gated ^{31}P NMR spectra of the equilibrium mixture after reaction of **[PdBr]** with $H(Et_2O)_2[B(C_6F_5)_4]$ (202 MHz, CD_2Cl_2).

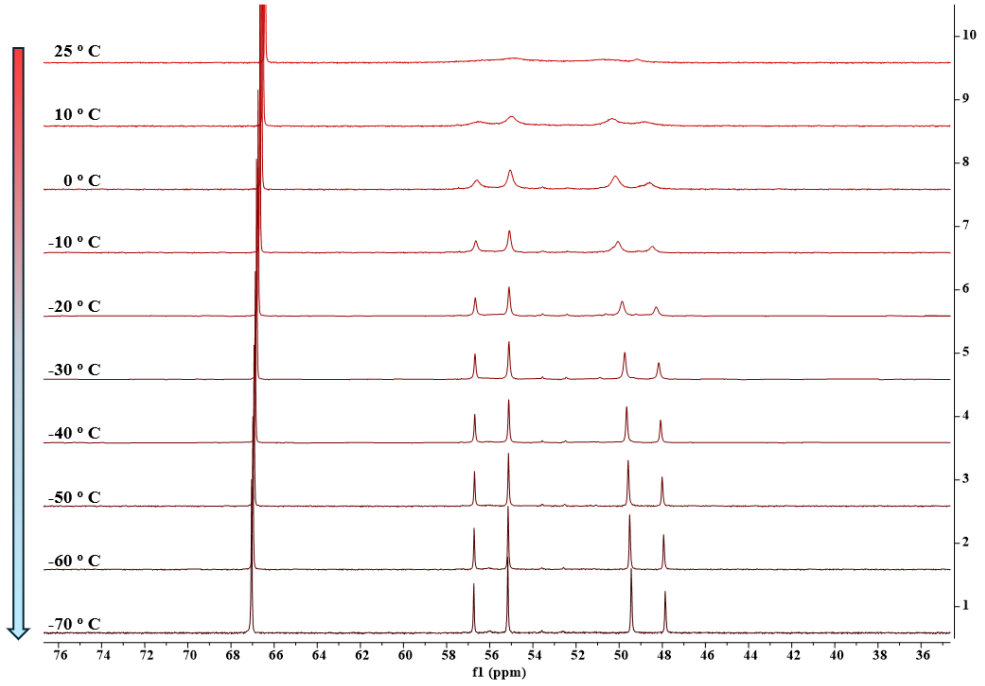

Figure S11- Variable temperature inverse-gated ^{31}P NMR spectra of the equilibrium mixture after reaction of

[PdBr] with $D(Et_2O)_2[B(C_6F_5)_4]$ (202 MHz, CD_2Cl_2).

EXSY Analysis

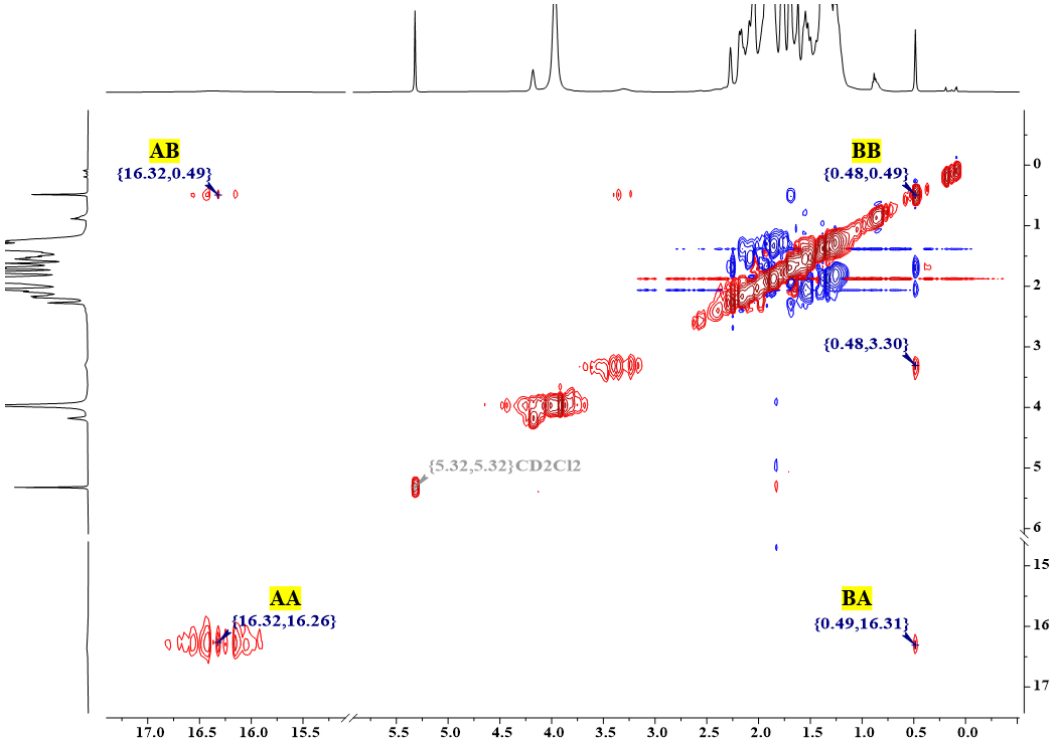

Figure S12- ^1H-^1H EXSY (red) – NOESY (blue) NMR spectrum of the equilibrium mixture after protonation of **[PdBr]** with $H(Et_2O)_2[B(C_6F_5)_4]$ (500, 500 MHz, CD_2Cl_2, 25 °C, τ_m = 0.5 s, NS = 64).

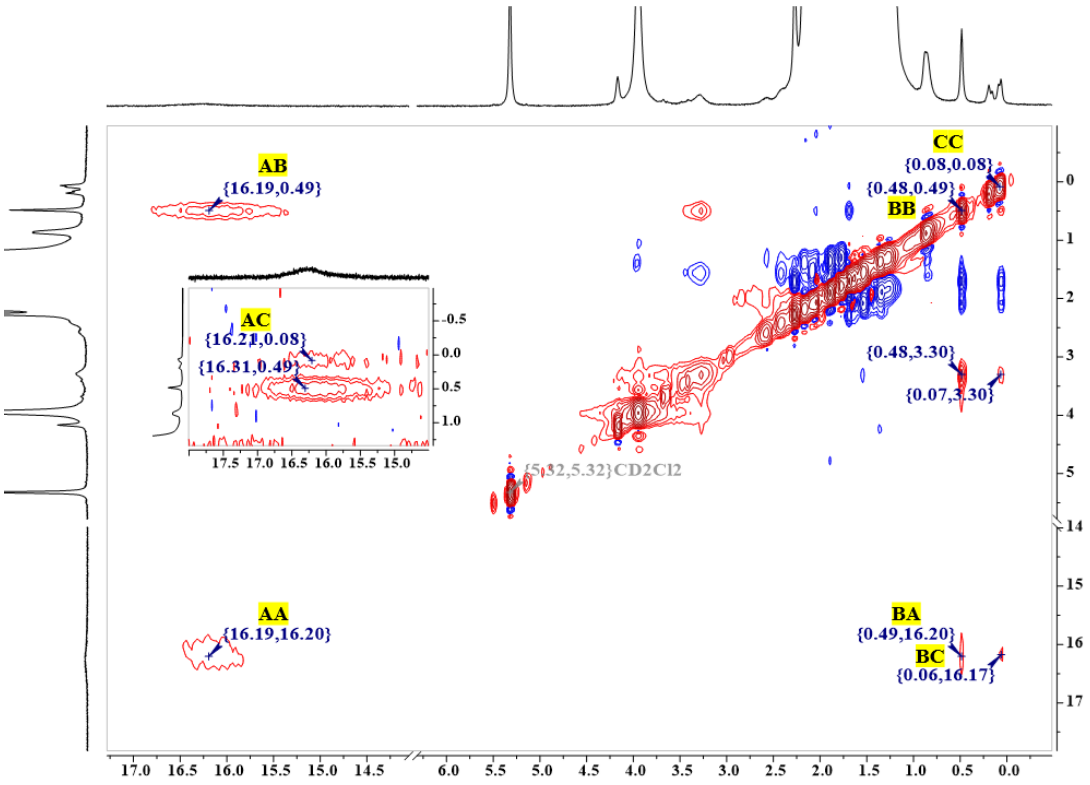

Figure S13- ^1H-^1H EXSY (red) – NOESY (blue) NMR spectrum of the equilibrium mixture after deuteration of **[PdBr]** with $D(Et_2O)_2[B(C_6F_5)_4]$ (500, 500 MHz, CD_2Cl_2, 25 °C, τ_m = 0.5 s, NS = 64).

Table S3- Calculation of the proton exchange rate constant between **[PdCH₂•Et₂O]⁺** and **[HBrH•2OEt₂]⁺** upon protonation from ^{1}H-^{1}H EXSY NMR data: AA (16.32, 16.26), AB (16.32, 0.49), BB (0.48, 0.49), BA (0.49, 16.31) and deuteration from ^{1}H-^{1}H EXSY NMR data: AA (16.19, 16.20), AB (16.19, 0.49), BB (0.48, 0.49), BA (0.49, 16.20)

	Mixing time τ_m (s)	*I*(AA)	*I*(AB)	*I*(BB)	*I*(BA)	Diagonal-peak to cross peak ratio (r)[a]	Rate constant *k* (s^{-1})[b]	$\Delta G^{\ddagger}_{298K}$ (kcal/mol)[c]
H⁺	0.5	0.4457	0.0613	1.0000	0.0712	10.91 ± 2.83	0.37 ± 0.74	22.27 ± 1.20
	1	0.2171	0.0782	1.0000	0.0888	7.29 ± 0.04	0.28 ± 0.01	22.44 ± 0.02
D⁺	0.5	0.1823	0.1338	1.0000	0.0374	6.91 ± 0.30	0.58 ± 0.13	21.99 ± 0.13
	0.75	0.2406	0.2402	1.0000	0.0655	4.06 ± 0.09	0.67 ± 0.05	21.91 ± 0.04

[a] $r = \frac{I\,(AA)+I\,(BB)}{I\,(AB)+I\,(BA)}$

[b] $k = \frac{1}{\tau_m} \ln\left(\frac{r+1}{r-1}\right)$.

[c] $\Delta G^{\ddagger} = -RT \ln\left(\frac{hk}{k_B T}\right)$ where R = gas constant, T = temperature (298 K), h = Planck's constant, k_B = Boltzmann's constant.

Addition of 2,4-dinitroaniline to [PdCH₂•Et₂O]⁺

*Addition of 2,4-dinitroaniline to the protonated **[PdCH₂•Et₂O]⁺**:* In the glovebox, the complex **[PdCH₂•Et₂O]⁺** was prepared as described above by protonation with $H(Et_2O)_2[B(C_6F_5)_4]$ and was dissolved in 0.6 mL CD_2Cl_2 in a J-Young tube. Then 2,4-dinitroaniline (2.2 mg, 0.012 mmol) was added to the J-Young tube. ^{1}H and ^{31}P NMR (Fig. S47-48) indicated that no reaction happened after mixing for one day. Then, the solvent was dried by applying high vacuum and the solid was redissolved in DCE. A sealed insert tube with acetone-d_6 was placed into the J.Young tube to improve locking/shimming. The ^{31}P NMR spectrum shows that no reaction was taken place in DCE indicating that 2,4-dinitroaniline is not a strong enough base to deprotonate **[PdCH₂•Et₂O]⁺**, therefore, the acidity of the **[PdCH₂•Et₂O]⁺** is weaker than the conjugate acid of 2,4-dinitroaniline (pK_{ip}^{DCE} = -3.9; pK_a^{THF} = -4.4 ± 0.5).

[H₃NAr^F][B(C₆F₅)₄]

Van't Hoff analysis (CD_2Cl_2)

In the glovebox, **[PdBr]** (7.4 mg, 0.01 mmol) and **[H₃NAr^F][B(C₆F₅)₄]** (8.1 mg, 0.01 mmol) were added in a J-Young tube. Then, 0.550 mL CD_2Cl_2 was added by a 1 mL micro-syringe, which gives the initial **[PdBr]** concentration c_i as 18 (± 3.9%) mmol/L. Then, the J. Young tube was capped. The solution color was very pale yellow after fully mixed. After 3h, ^{31}P{^{1}H} NMR was collected from -70 ºC to 25 ºC with 10 ºC intervals between each spectrum. The ^{31}P signal at 52.7 ppm is proposed to be the acid-base adduct **[PdBr•H₃N^F]⁺**. The concentration of **[PdBr•H₃N^F]⁺** (c(PdBr•H_3N^F)) and **[Pd-Br-Pd]⁺** (c(Pd-Br-Pd)) were calculated using equation S5-6 with their integration I(PdBr•H_3N^F) and I(Pd-Br-Pd) relative to the sum of all ^{31}P signals originating from initial **[PdBr]** added to the reaction (c_i). Errors were calculated using standard error propagation. K_2 was calculated at all temperatures based on the ^{31}P NMR

by using equation S4. Van't Hoff plot was made with lnK_2 versus 1000/T, which allowed the calculation of experimental thermodynamic values for the equilibrium K_2.

An independent experiment conducted in an identical condition in DCE showed that no **[PdCH$_2$•H$_2$N^F]$^+$** was formed even though spinning the NMR tube on a rotating stirrer for two days. The experiments in both DCM and DCE indicate that **[H$_3$NAr^F][B(C$_6$F$_5$)$_4$]** is not a strong enough acid to protonate **[PdBr]**. Therefore, the acidity of the **[PdCH$_2$]$^+$** is stronger than **[H$_3$NAr^F][B(C$_6$F$_5$)$_4$]** (pK_{ip}^{DCE} = 4.4 ± 0.5; pK_a^{THF} = 3.8 ± 0.5).

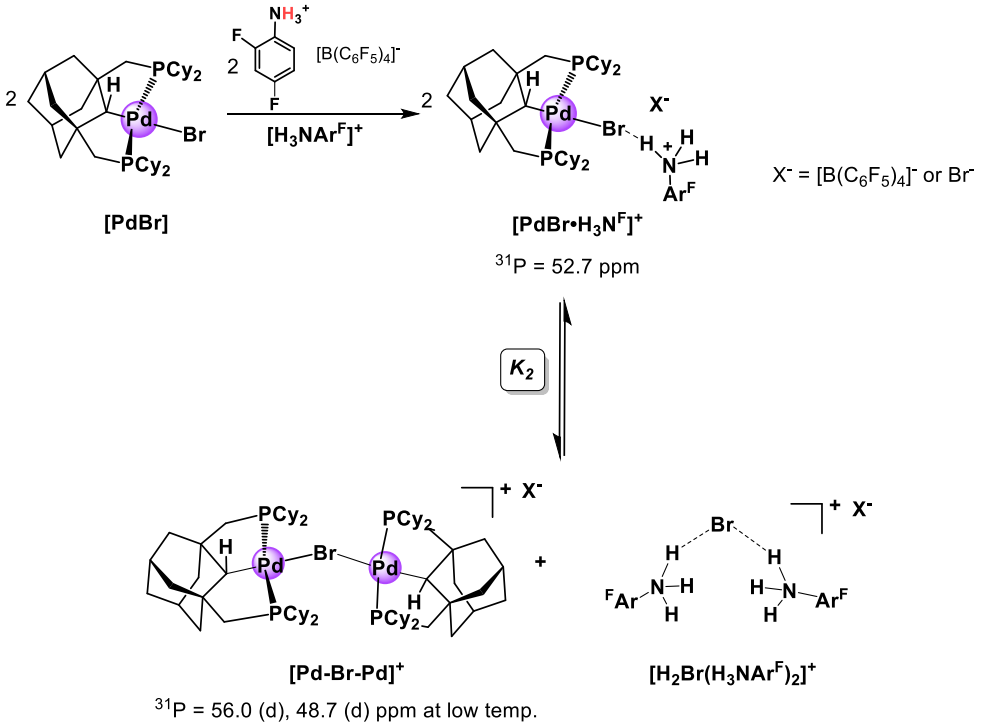

Scheme S2- Proposed equilibrium processed upon addition of **[H$_3$NAr^F][B(C$_6$F$_5$)$_4$]** to **[PdBr]**.

$$K_2 = \frac{c(\text{Pd-Br-Pd})^2}{c(\text{PdBr•H}_3\text{N}^F)^2} \tag{S4}$$

$$c(\text{PdBr•H}_3\text{N}^F) = \frac{I(\text{PdBr•H}_3\text{N}^F)}{0.5\, I(\text{Pd-Br-Pd}) + I(\text{PdBr•H}_3\text{N}^F)} \times c_i \tag{S5}$$

$$c(\text{Pd-Br-Pd}) = \frac{0.5\, I(\text{Pd-Br-Pd})}{0.5\, I(\text{Pd-Br-Pd}) + I(\text{PdBr•H}_3\text{N}^F)} \times c_i \tag{S6}$$

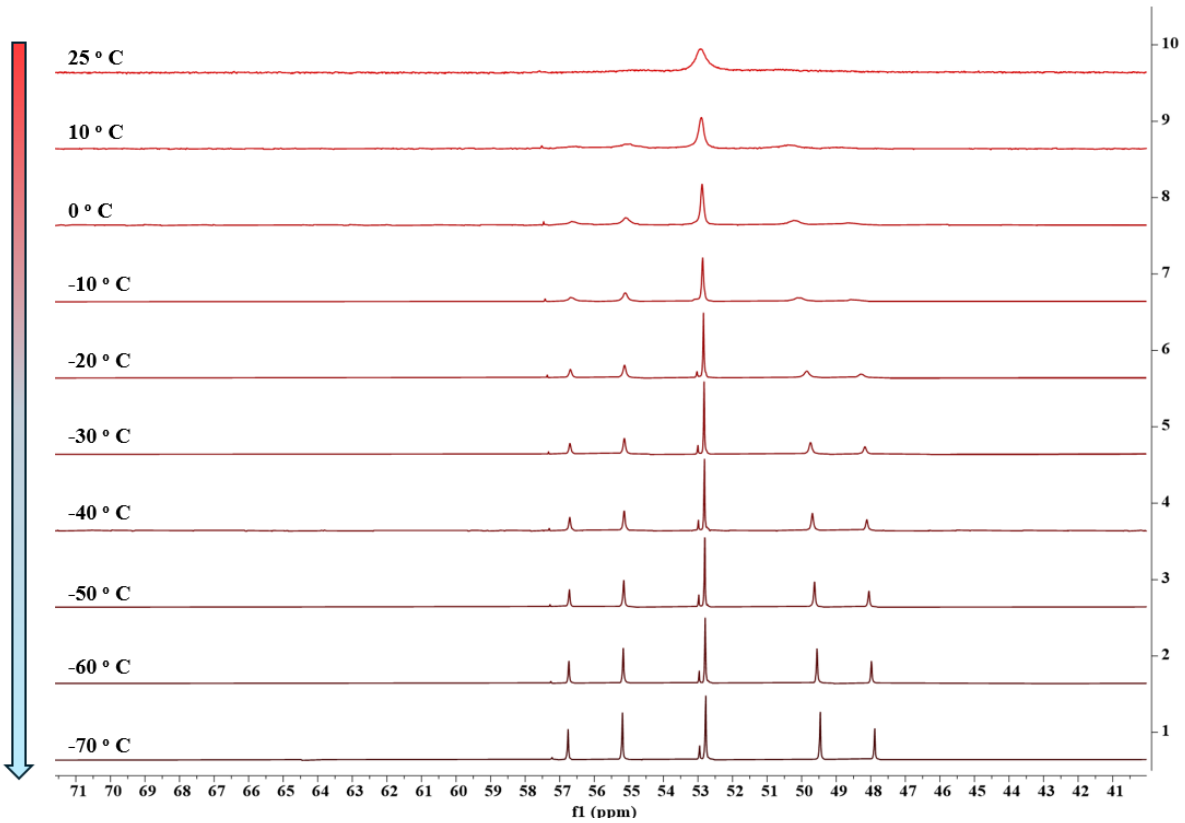

Figure S14- Variable temperature inverse-gated ^{31}P NMR (202 MHz, CD_2Cl_2) spectrum of the equilibrium mixture after addition of **[H_3NAr^F][$B(C_6F_5)_4$]** to **[PdBr]**.

Table S4- Integration of **[PdBr•H_3N^F]$^+$** (I(PdBr•H_3N^F)), **[Pd-Br-Pd]$^+$** (I(Pd-Br-Pd)), K_2, and Ln K_2 from 10 ºC to -20 ºC upon addition of **[H_3NAr^F][$B(C_6F_5)_4$]** to **[PdBr]** in CD_2Cl_2.

T(ºC)	I(Pd-Br-Pd)	I(CH•H_3N^F)	K_2 * 10^1	Ln K_2
10	1.07 (14)	1.00	2.86 (96)	-1.25 (33)
0	1.36 (11)	1.00	4.62 (95)	-0.77 (21)
-10	1.50 (9)	1.00	5.62 (93)	-0.58 (17)
-20	1.75 (6)	1.00	7.66 (86)	-0.27 (11)

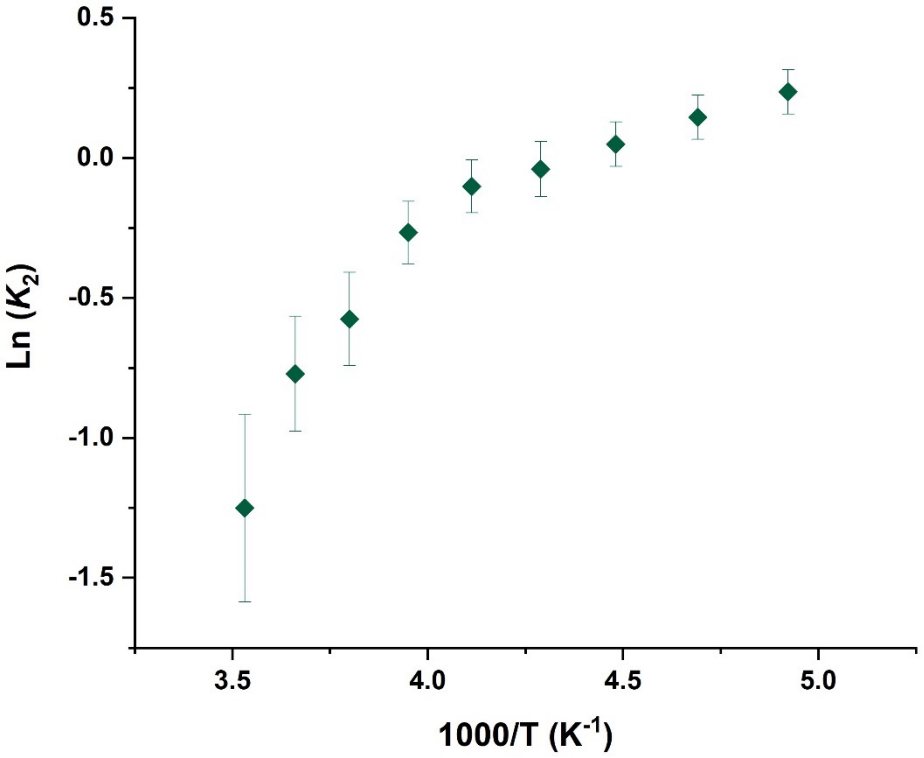

Figure S15- Full region of the Van't Hoff plot for the reaction of **[H_3NAr^F][$B(C_6F_5)_4$]** and **[PdBr]** in CD_2Cl_2

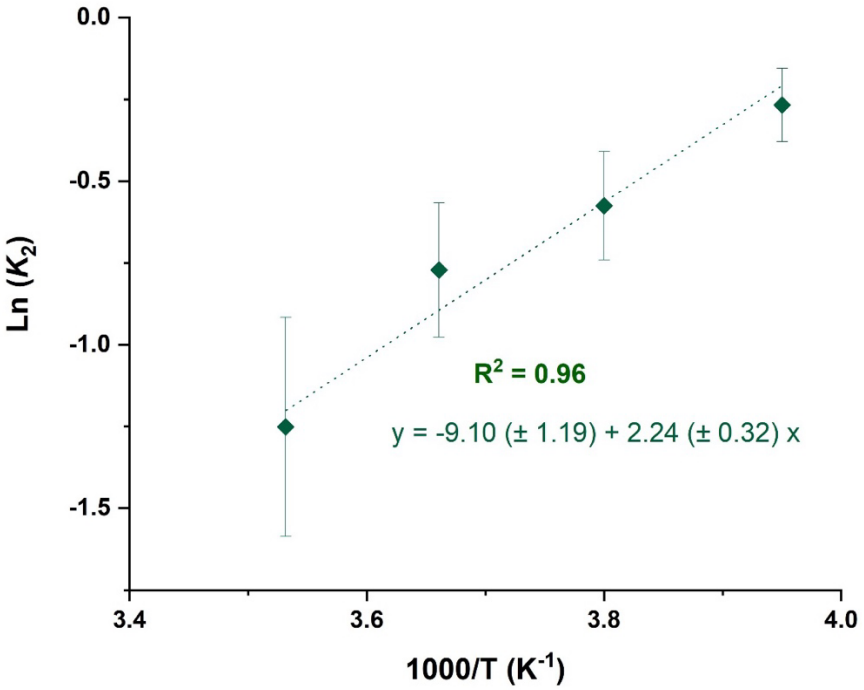

Figure S16- Linear region of the Van't Hoff plot for the reaction of **[H_3NAr^F][$B(C_6F_5)_4$]** and **[PdBr]** in CD_2Cl_2.

Table S5- Experimental thermodynamic values for the equilibrium upon addition of **[H_3NAr^F][$B(C_6F_5)_4$]** to **[PdBr]** in CD_2Cl_2.

	ΔH (kcal/mol)	ΔS (cal/(mol·K))	ΔG_{298K} (kcal/mol)
K_2	-4.49 ± 0.64	-18.21 ± 2.38	0.94 ± 0.95

EXSY analysis (CD_2Cl_2)

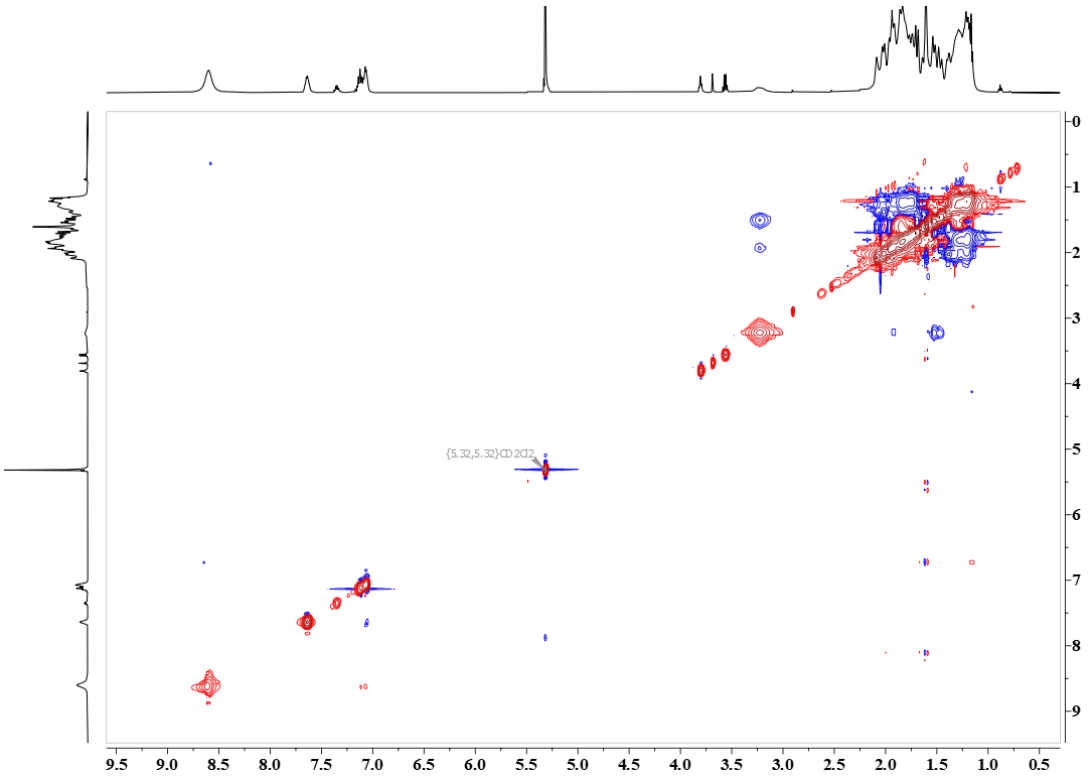

Figure S17- Section of 1H-1H EXSY (red) -NOESY(blue) NMR spectrum of the equilibrium mixture after protonation of **[PdBr]** with **[H_3NAr^F][$B(C_6F_5)_4$]** (500, 500 MHz, CD_2Cl_2, 25 °C, τ_m = 0.5 s, NS = 64).

[H_3NAr^{Cl}][$B(C_6F_5)_4$]

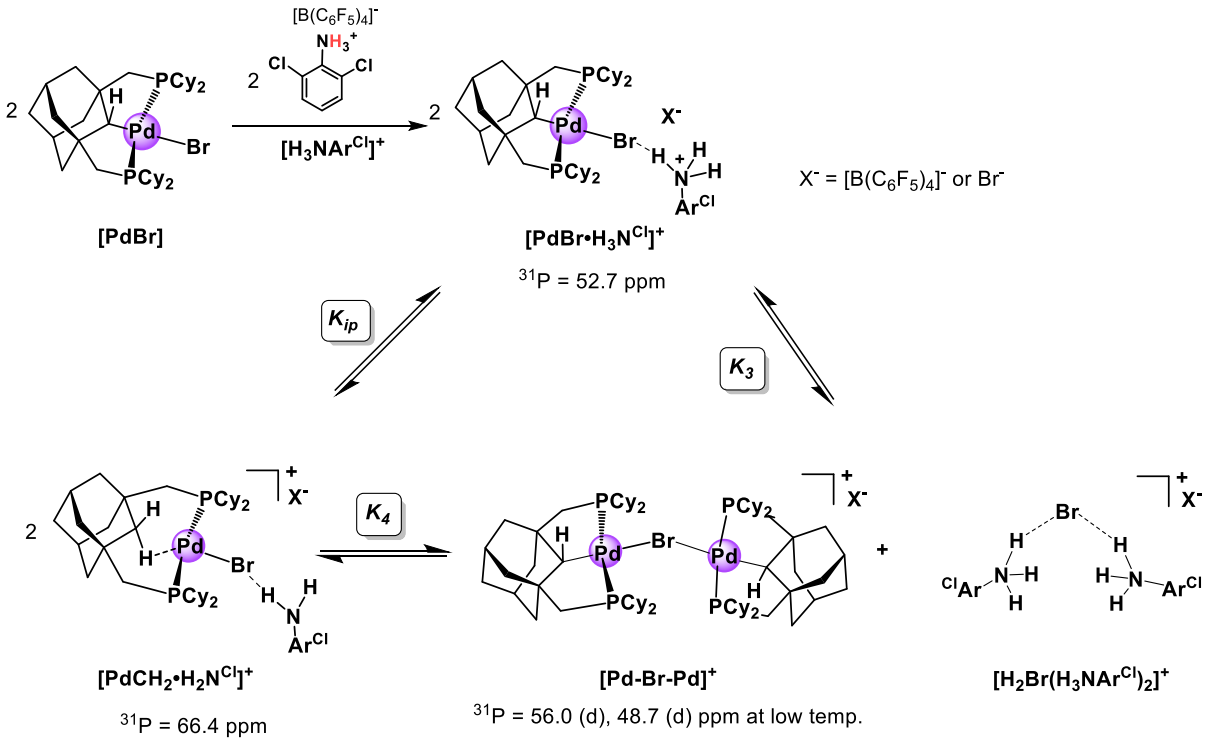

Scheme S3- Proposed equilibrium processed upon addition of [H_3NAr^{Cl}][$B(C_6F_5)_4$] to **[PdBr]**.

$$c(\mathrm{PdCH_2{\bullet}H_2N^{Cl}}) = \frac{I(\mathrm{PdCH_2{\bullet}H_2N^{Cl}})}{0.5\,I(\text{Pd-Br-Pd}) + I(\mathrm{PdCH_2{\bullet}H_2N^{Cl}}) + I(\mathrm{PdBr{\bullet}H_3N^{Cl}})} \times c_i \quad \text{(S7)}$$

$$c(\mathrm{PdBr{\bullet}H_2N^{Cl}}) = \frac{I(\mathrm{PdBr{\bullet}H_3N^{Cl}})}{0.5\,I(\text{Pd-Br-Pd}) + I(\mathrm{PdCH_2{\bullet}H_2N^{Cl}}) + I(\mathrm{PdBr{\bullet}H_3N^{Cl}})} \times c_i \quad \text{(S8)}$$

$$c(\text{Pd-Br-Pd}) = \frac{0.5\,I(\text{Pd-Br-Pd})}{0.5\,I(\text{Pd-Br-Pd}) + I(\mathrm{PdCH_2{\bullet}H_2N^{Cl}}) + I(\mathrm{PdBr{\bullet}H_3N^{Cl}})} \times c_i \quad \text{(S9)}$$

$$K_3 = \frac{c(\text{Pd-Br-Pd})^2}{c(\mathrm{PdBr{\bullet}H_3NCl})^2} \quad \text{(S10)}$$

$$K_4 = \frac{c(\text{Pd-Br-Pd})^2}{c(\mathrm{PdCH_2{\bullet}H_2N^{Cl}})^2} \quad \text{(S11)}$$

$$K_{ip} = \frac{c(\mathrm{PdBr{\bullet}H_3N^{Cl}})^2}{c(\mathrm{PdCH_2{\bullet}H_2N^{Cl}})^2} \quad \text{(S12)}$$

Van't Hoff analysis (DCE)

In the glovebox, **[PdBr]** (8.2 mg, 0.011 mmol) and **[H_3NAr^{Cl}][$B(C_6F_5)_4$]** (9.3 mg, 0.011 mmol) were added in a J-Young tube. Then, 0.55 mL DCE was added by a 1 mL micro-syringe, which gives the initial **[PdBr]** concentration c_i as 20 (± 3.8%) mmol/L. Then, the J. Young tube was capped. The solution color turned brown after fully mixed. After 30 mins, $^{31}P\{^1H\}$ NMR was collected from -15 ºC to 25 ºC with 5 ºC intervals between each spectrum. The ^{31}P signal at 52.7 ppm is proposed to be the acid-base adduct **[$PdBr{\bullet}H_3N^{Cl}$]$^+$**. The concentration of **[$PdCH_2{\bullet}H_2N^{Cl}$]$^+$** ($c(PdCH_2{\bullet}H_2N^{Cl})$), **[$PdBr{\bullet}H_3N^{Cl}$]$^+$**

(c(PdBr•H_3N^{Cl})) and **[Pd-Br-Pd]$^+$** (c(Pd-Br-Pd)) were calculated using equation S7-9 with their integration I($PdCH_2$•H_2N^{Cl}), I(PdBr•H_3N^{Cl}) and I(Pd-Br-Pd) relative to the sum of all ^{31}P signals originating from initial **[PdBr]** added to the reaction (c_i). Error was calculated using standard error propagation. K_3, K_4 and K_{ip} were calculated at all temperatures based on the ^{31}P NMR by using equation S10-12. Therefore, we estimated that pK_{ip}^{DCE} of **[PdCH$_2$]$^+$** is -1.0 ± 0.5 using equation S13 with K_{ip} = 1.15 (± 0.27) x 10^2 at 25 ºC. The pK_a^{MeCN}, and pK_a^{THF} were calculated using equations S14-15[10, 11]. Van't Hoff plots are made for K_3, K_4 and K_{ip} with their corresponding lnK_{eq} versus 1000/T, which allows the calculation of experimental thermodynamic values for the equilibrium processes.

$$pK_{ip}\ ([PdCH_2]^+, DCE) = pK_{ip}\ ([H_3NAr^{Cl}][B(C_6F_5)_4], DCE) - \log K_{ip} \quad (S13)$$

$$pK_{ip}\ (DCE) = pK_a\ (MeCN) \bullet 0.99 - 3.93 \quad (S14)$$

$$pK_a\ (THF) = pK_a\ (MeCN) \bullet (0.98 \pm 0.02) - (6.1 \pm 0.4) + 2 \bullet (0.84 \pm 0.16) \quad (S15)$$

Table S6- acidity of anilinium acids and the calculated acidity of **[PdCH$_2$]$^+$** in MeCN, DCE and THF.

	2,4-dinitroanilinium	**[H_3NAr^F][$B(C_6F_5)_4$]**	**[H_3NAr^{Cl}][$B(C_6F_5)_4$]**	**[$PdCH_2$]$^+$**
pK_a^{MeCN}	0.03[b]	8.39	5.07	2.9 ± 0.5[b]
pK_{ip}^{DCE}	-3.9	4.4 ± 0.5[b]	1.1 ± 0.5[b]	-1.0 ± 0.5[a]
pK_a^{THF}	-4.4 ± 0.5[c]	3.8 ± 0.5[c]	0.6 ± 0.5[c]	-1.6 ± 0.7[c]

[a] calculated with equation S13

[b] calculated with equation S14

[c] calculated with equation S15

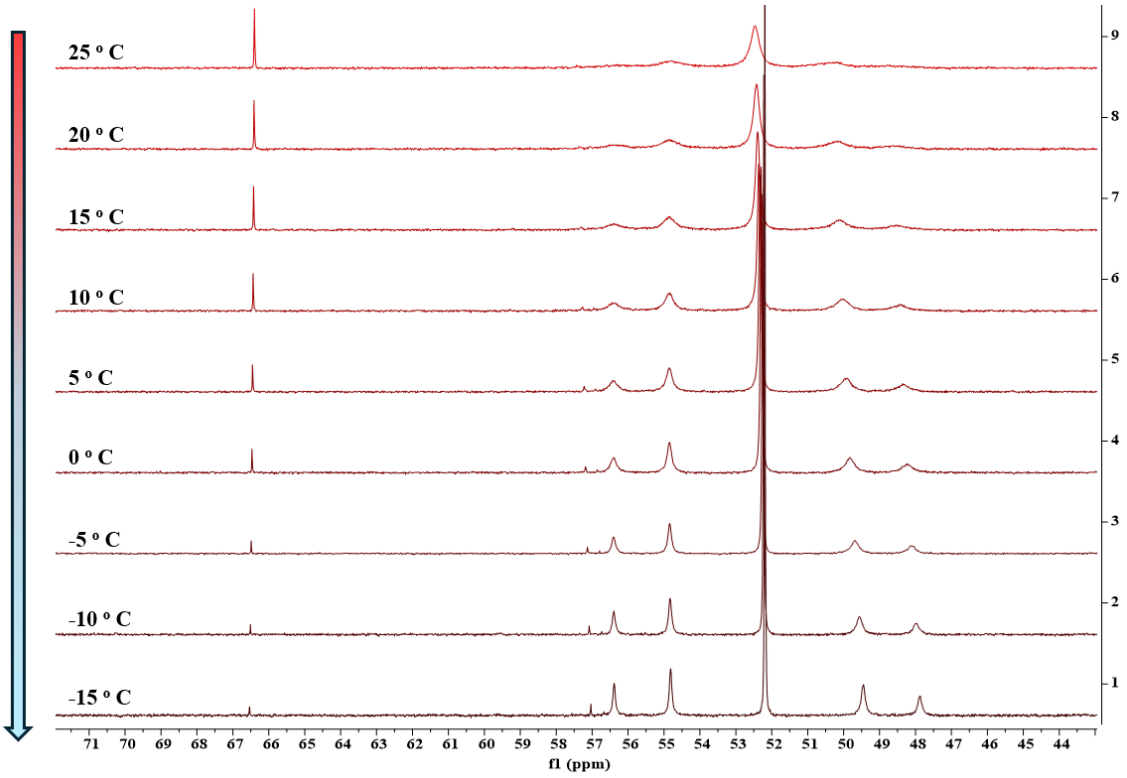

Figure S18- Variable temperature inverse-gated ^{31}P NMR (202 MHz, DCE) spectrum of the equilibrium mixture after addition of **[H_3NAr^{Cl}][$B(C_6F_5)_4$]** to **[PdBr]**.

Table S7- Integration of **[PdCH$_2$•H$_2$N^{Cl}]$^+$** (*I*(PdCH$_2$•H$_2$N^{Cl})), **[PdBr•H$_3$N^{Cl}]$^+$** (*I*(PdBr•H$_3$N^{Cl})), **[Pd-Br-Pd]$^+$** (*I*(Pd-Br-Pd)), K_3, K_4, K_{ip}, Ln K_3, Ln K_4 and Ln K_{ip} from 25 ºC to -15 ºC upon addition of **[H$_3$NAr^{Cl}][B(C$_6$F$_5$)$_4$]** to **[PdBr]** in DCE.

T(ºC)	*I*([CH$_2$PdBr •H$_2$NAr^{Cl}]$^+$)	*I*(Pd-Br-Pd)	I([CHPdBr •H$_3$NAr^{Cl}]$^+$)	K_3 * 10^1	Ln K_3	K_4	Ln K_4	K_{ip} * 10^{-2}	Ln K_{ip}
25	1.00 (2)	12.67 (1.94)	10.73	3.48 (1.10)	-1.05 (31)	40.13 (12.71)	3.69 (32)	1.15 (27)	4.75 (23)
20	1.00 (2)	15.86 (1.75)	13.65	3.38 (79)	-1.09 (23)	62.88 (14.83)	4.14 (24)	1.86 (33)	5.23 (18)
15	1.00 (3)	17.35 (1.69)	15.24	3.24 (67)	-1.13 (21)	75.26 (16.04)	4.32 (21)	2.32 (38)	5.45 (16)
10	1.00 (4)	23.87 (2.05)	22.42	2.83 (52)	-1.26 (18)	142.44 (27.30)	4.96 (19)	5.03 (75)	6.22 (15)
5	1.00 (3)	27.5 (1.96)	27.34	2.53 (40)	-1.37 (16)	189.06 (31.15)	5.24 (16)	7.47 (97)	6.62 (13)
0	1.00 (4)	31.55 (1.83)	33.69	2.19 (29)	-1.52 (13)	248.85 (36.59)	5.52 (14)	11.35 (1.36)	7.03 (12)
-5	1.00 (5)	42.70 (2.22)	48.89	1.91 (24)	-1.66 (12)	455.82 (65.59)	6.12 (14)	23.90 (2.96)	7.78 (12)
-10	1.00 (11)	48.85 (3.13)	59.79	1.67 (23)	-1.79 (14)	596.58 (126.01)	6.39 (21)	35.75 (6.82)	8.18 (19)
-15	1.00 (17)	62.66 (2.55)	73.59	1.81 (20)	-1.71 (11)	981.57 (257.71)	6.89 (26)	54.15 (13.87)	8.60 (26)

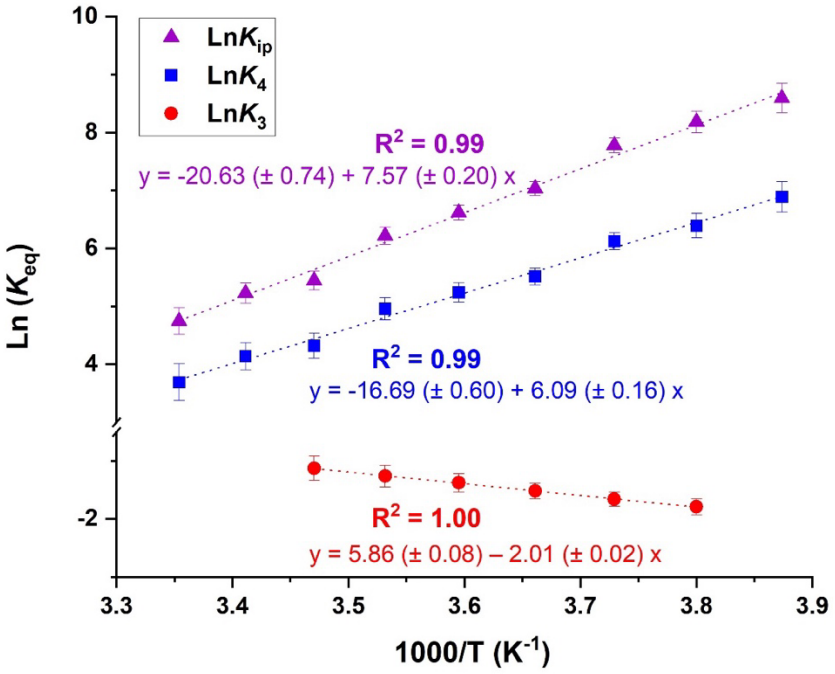

Figure S19- Van't Hoff plot for the reaction of **[H$_3$NAr^{Cl}][B(C$_6$F$_5$)$_4$]** and **[PdBr]** in DCE.

Table S8- Experimental thermodynamic values for the equilibrium upon addition of **[H$_3$NAr^{Cl}][B(C$_6$F$_5$)$_4$]** to **[PdBr]** in DCE.

	ΔH (kcal/mol)	ΔS (cal/(mol·K))	ΔG_{298K} (kcal/mol)
K_3	4.03 ± 0.05	11.72 ± 0.17	0.54 ± 0.07
K_4	-12.18 ± 0.33	-33.38 ± 1.19	-2.23 ± 0.48
K_{ip}	-15.14 ± 0.41	-41.27 ± 1.47	-2.84 ± 0.60

Van't Hoff analysis (CD_2Cl_2)

In the glovebox, **[PdBr]** (7.4 mg, 0.01 mmol) and **[H_3NAr^{Cl}][$B(C_6F_5)_4$]** (8.4 mg, 0.01 mmol) were added in a J-Young tube. Then, 0.550 mL CD_2Cl_2 was added by a 1 mL micro-syringe, which gives the initial **[PdBr]** concentration c_i as 18 (± 3.9%) mmol/L. Then, the J. Young tube was capped. The solution color turned brown after fully mixed. After 1.5h, inverse-gated $^{31}P\{^1H\}$ NMR was collected from -70 ºC to 25 ºC with 10 ºC intervals between each spectrum (Fig. S20). The relative error of the integration of the peaks at 48.7 ppm and 66.4 ppm in ^{31}P NMR spectrum were obtained by the reciprocal for their S/N (signal/noise), which were the main contribution to the spectrum error. The ^{31}P signal at 52.7 ppm was proposed to be the acid-base adduct **[PdBr•H_3N^{Cl}]$^+$**. The concentration of **[$PdCH_2$•H_2N^{Cl}]$^+$** (c($PdCH_2$•H_2N^{Cl})), **[PdBr•H_3N^{Cl}]$^+$** (c(PdBr•H_3N^{Cl})) and **[Pd-Br-Pd]$^+$** (c(Pd-Br-Pd)) were calculated using equation S7-9 with their integration I($PdCH_2$•H_2N^{Cl}), I(PdBr•H_3N^{Cl}) and I(Pd-Br-Pd) relative to the sum of all ^{31}P signals originating from initial **[PdBr]** added to the reaction (c_i). Error was calculated using standard error propagation. K_3, K_4 and K_{ip} were calculated at all temperatures based on the ^{31}P NMR by using equation S10-12. Van't Hoff plot was made for K_3, K_4 and K_{ip} with their corresponding lnK_{eq} versus 1000/T, which allowed the calculation of experimental thermodynamic values for the equilibrium processes. Van't Hoff plots were made from 10 ºC to -30 ºC, where the intensity of the peak at 66.4 ppm allows accurate integration.

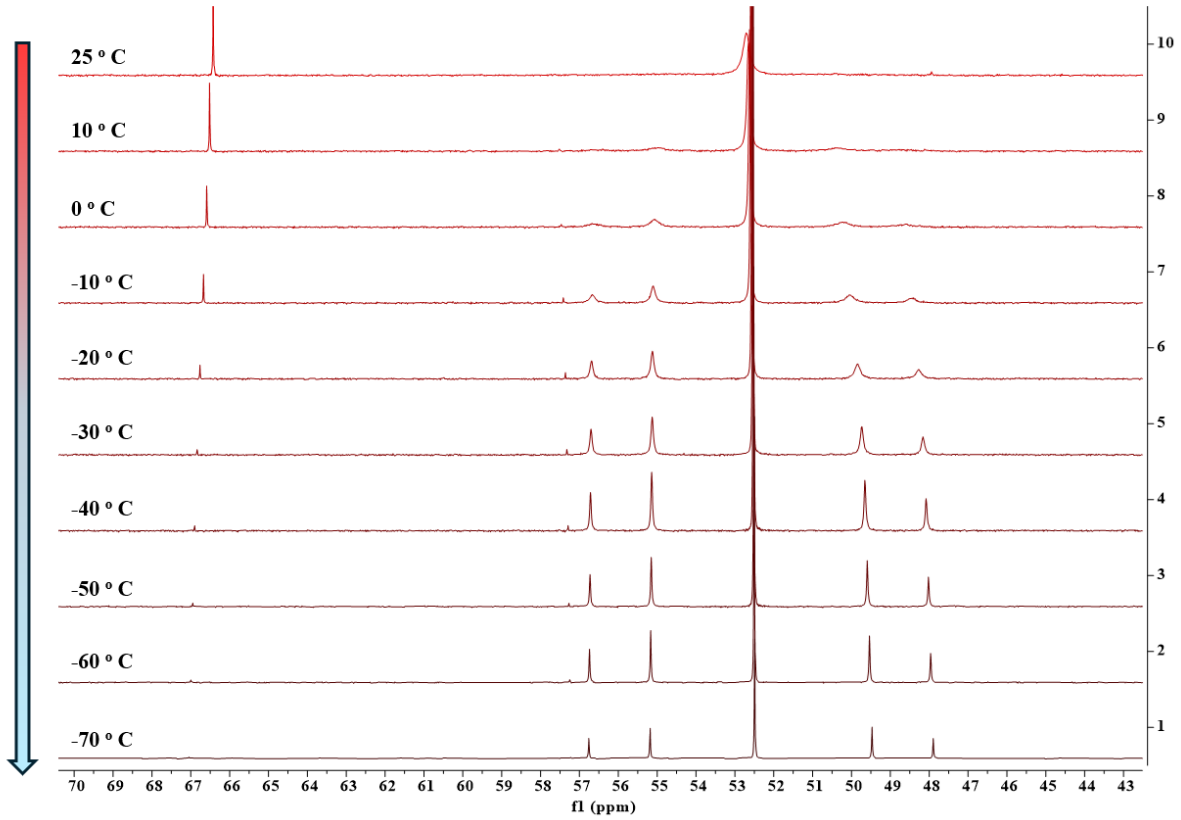

Figure S20- Variable temperature inverse-gated ^{31}P NMR (202 MHz, CD_2Cl_2) spectrum of the equilibrium mixture after addition of **[H_3NAr^{Cl}][$B(C_6F_5)_4$]** to **[PdBr]**.

Table S9- Integration of **[PdCH$_2$•H$_2$N^{Cl}]$^+$** (*I*(PdCH$_2$•H$_2$N^{Cl})), **[PdBr•H$_3$N^{Cl}]$^+$** (*I*(PdBr•H$_3$N^{Cl})), **[Pd-Br-Pd]$^+$** (*I*(Pd-Br-Pd)), K_3, K_4, K_{ip}, Ln K_3, Ln K_4 and Ln K_{ip} from 10 ºC to -30 ºC upon addition of **[H$_3$NAr^{Cl}][B(C$_6$F$_5$)$_4$]** to **[PdBr]** in CD_2Cl_2.

T(ºC)	*I*(|CH$_2$PdBr •H$_2$NAr^{Cl}|$^+$)	*I*(Pd-Br-Pd)	I(|CHPdBr•H$_3$NAr^{Cl}|$^+$)	K_3 * 10^2	Ln K_3	K_4	Ln K_4	K_{ip} * 10^{-2}	Ln K_{ip}
10	1.00 (2)	5.01 (1.12)	10.70	5.48 (1.99)	-2.90 (36)	6.28 (2.28)	1.84 (36)	1.14 (20)	4.74 (18)
0	1.00 (2)	9.38 (1.48)	16.85	7.75 (2.10)	-2.56 (27)	22.00 (6.01)	3.09 (27)	2.84 (44)	5.65 (16)
-10	1.00 (3)	19.9 (1.96)	31.46	10.00 (1.85)	-2.30 (18)	99.00 (18.71)	4.60 (19)	9.90 (1.26)	6.90 (13)
-20	1.00 (7)	44.53 (2.24)	60.75	13.43 (1.59)	-2.01 (12)	495.73 (77.07)	6.21 (16)	36.90 (5.10)	8.21 (14)
-30	1.00 (17)	121.63 (3.27)	150.15	16.40 (1.50)	-1.81 (9)	3698.46 (970.83)	8.22 (26)	225.45 (58.56)	10.02 (26)

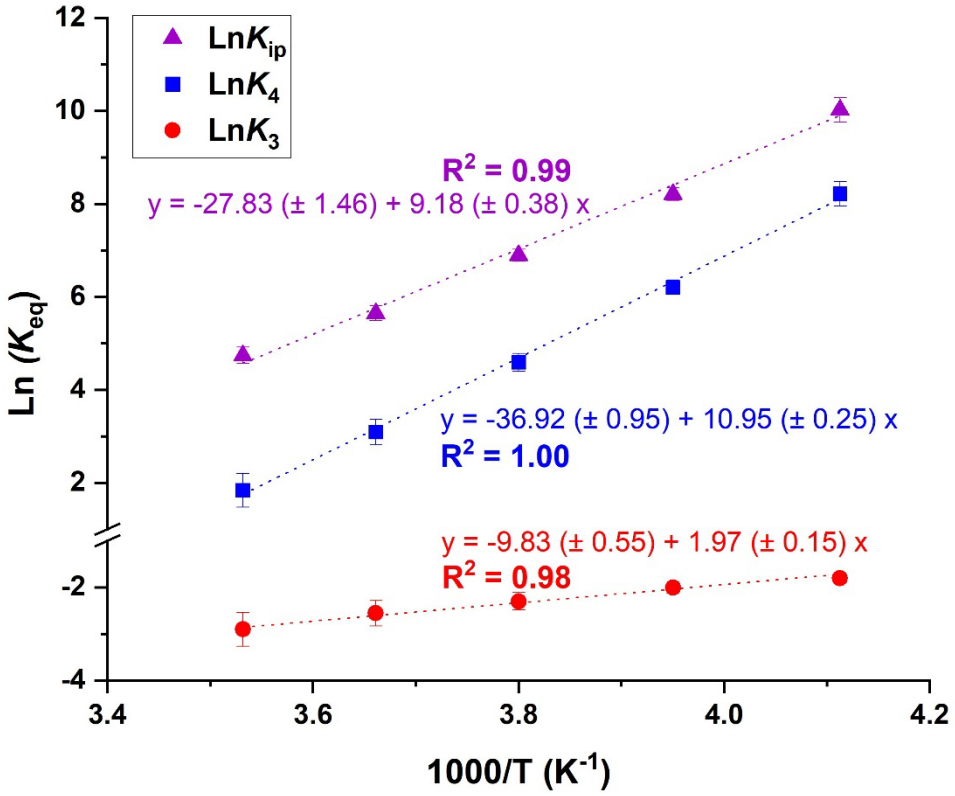

Figure S21- Van't Hoff plot for the reaction of **[H$_3$NAr^{Cl}][B(C$_6$F$_5$)$_4$]** and **[PdBr]** in CD_2Cl_2.

Table S10- Experimental thermodynamic values for the equilibrium upon addition of **[H$_3$NAr^{Cl}][B(C$_6$F$_5$)$_4$]** to **[PdBr]** in CD_2Cl_2.

	Δ*H* (kcal/mol)	Δ*S* (cal/(mol·K))	ΔG_{298K} (kcal/mol)
K_3	-3.94 ± 0.30	-19.66 ± 1.10	1.91 ± 0.44
K_4	-21.90 ± 0.50	-73.84 ± 1.89	0.10 ± 0.75
K_{ip}	-18.35 ± 0.76	-55.67 ± 2.91	-1.76 ± 1.15

EXSY analysis (CD_2Cl_2)

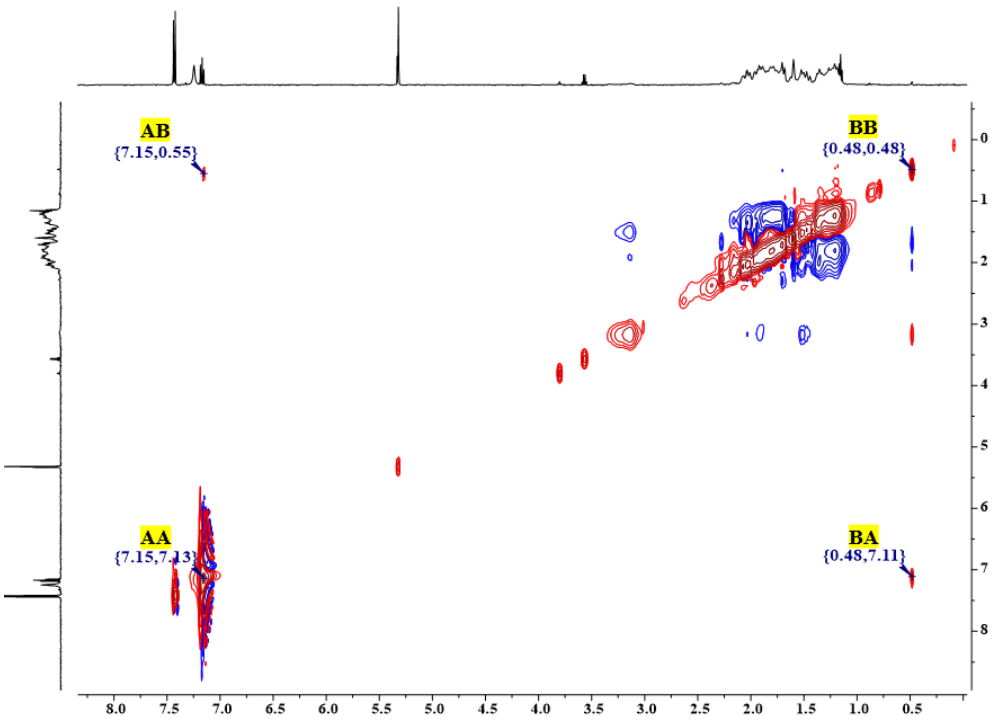

Figure S22- Section of ^{1}H-^{1}H EXSY (red) -NOESY(blue) NMR spectrum of the equilibrium mixture after protonation of **[PdBr]** with **[H_3NAr^{Cl}][$B(C_6F_5)_4$]** (500, 500 MHz, CD_2Cl_2, 25 °C, τ_m = 0.5 s, NS = 64).

Table S11- Calculation of the proton exchange rate constant between **[PdBr•H_3N^{Cl}]$^+$** and **[$PdCH_2$•H_2N^{Cl}]$^+$** from ^{1}H-^{1}H EXSY NMR data. AA (7.15, 7.13), AB (7.15, 0.55), BB (0.48, 0.48), BA (0.48, 7.11).

Mixing time τ_m (s)	***I*(AA)**	***I*(AB)**	***I*(BB)**	***I*(BA)**	**Diagonal-peak to cross peak ratio (r)[a]**	**Rate constant *k* (s^{-1})[b]**	**$\Delta G^{\ddagger}_{298}$ (kcal/mol)[c]**
0.5	1	0.0069	0.083	0.0143	51.08 (9.54)	0.078 (0.529)	23.2 (4.0)

[a] $r = \frac{I\,(AA)+I\,(BB)}{I\,(AB)+I\,(BA)}$

[b] $= \frac{1}{\tau_m} \ln\left(\frac{r+1}{r-1}\right)$.

[c] $\Delta G^{\ddagger}$ = -RT ln $\left(\frac{hk}{k_B T}\right)$ where R = gas constant, T = temperature (298K), h = Planck's constant, k_B = Boltzmann's constant.

Table S12- Summary of experimental thermodynamic values for the equilibrium processes K_1, K_2, K_3, K_4 and K_{ip}.

		ΔH (kcal/mol)	ΔS (cal/(mol·K))	ΔG_{298K} (kcal/mol)
K_1	H^+	-1.42 ± 0.05	-5.44 ± 0.20	0.20 ± 0.08
	D^+	-3.47 ± 0.20	-13.39 ± 0.69	0.52 ± 0.29
K_2	CD_2Cl_2	-4.49 ± 0.64	-18.21 ± 2.38	0.94 ± 0.95
K_3	CD_2Cl_2	-3.94 ± 0.30	-19.66 ± 1.10	1.91 ± 0.44
	DCE	4.03 ± 0.05	11.72 ± 0.17	0.54 ± 0.07
K_4	CD_2Cl_2	-21.90 ± 0.50	-73.84 ± 1.89	0.10 ± 0.75
	DCE	-12.18 ± 0.33	-33.38 ± 1.19	-2.23 ± 0.48
K_{ip}	CD_2Cl_2	-18.35 ± 0.76	-55.67 ± 2.91	-1.76 ± 1.15
	DCE	-15.14 ± 0.41	-41.27 ± 1.47	-2.84 ± 0.60

NMR Spectra

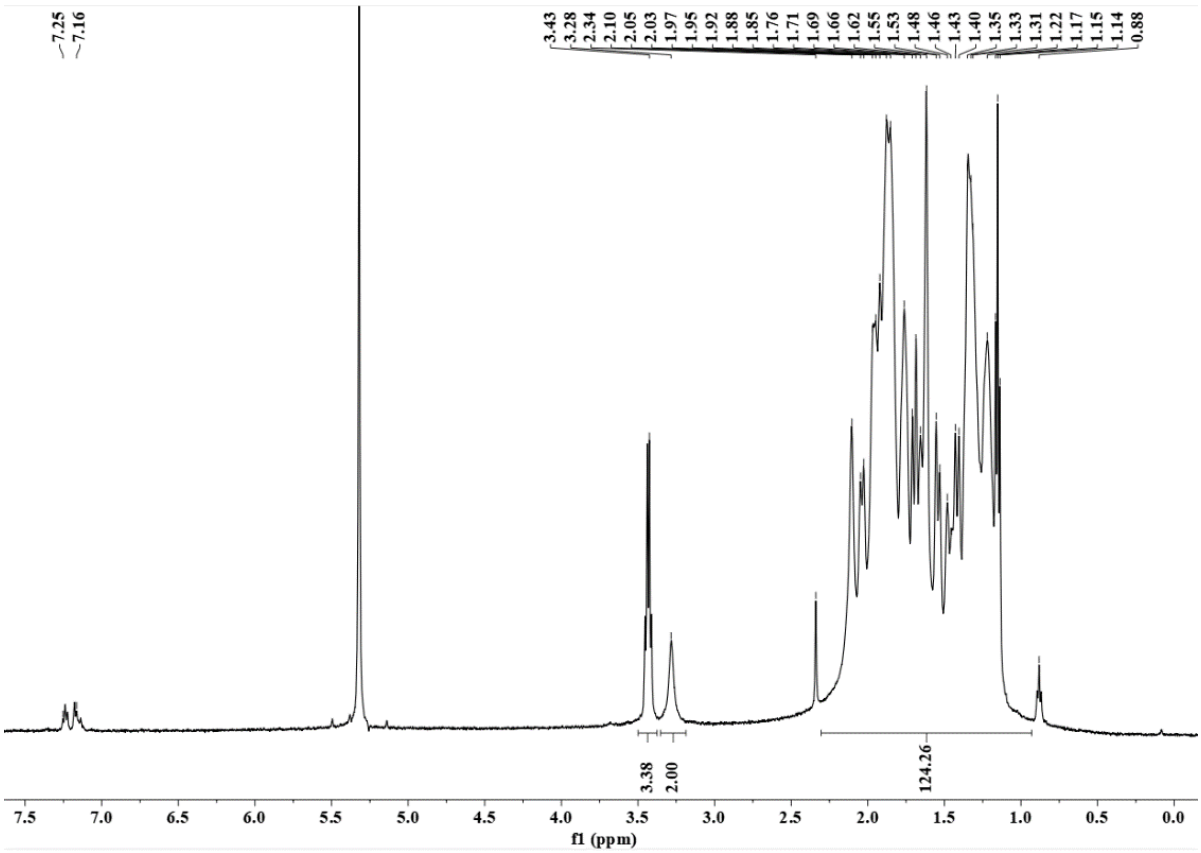

Figure S23- ^{1}H NMR spectrum of **[Pd-Br-Pd]$^+$** (500 MHz, CD_2Cl_2, 25 °C). Signals at 7.25, 7.16 and 2.34 ppm are residual toluene, 3.43 and 1.15 ppm are residual Et_2O, and 0.88 ppm is pentane.

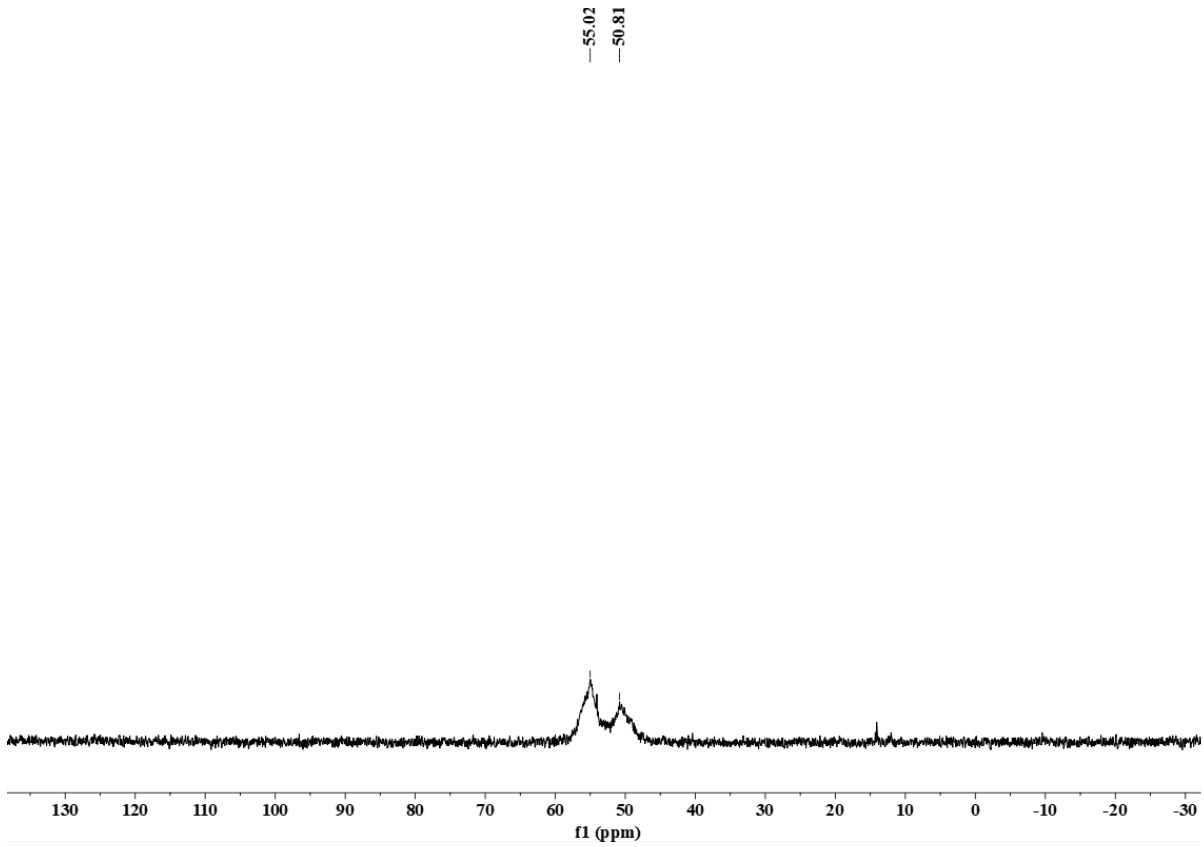

Figure S24- ^{31}P NMR spectrum of **[Pd-Br-Pd]**$^{+}$ (202 MHz, CD_2Cl_2, 25 °C).

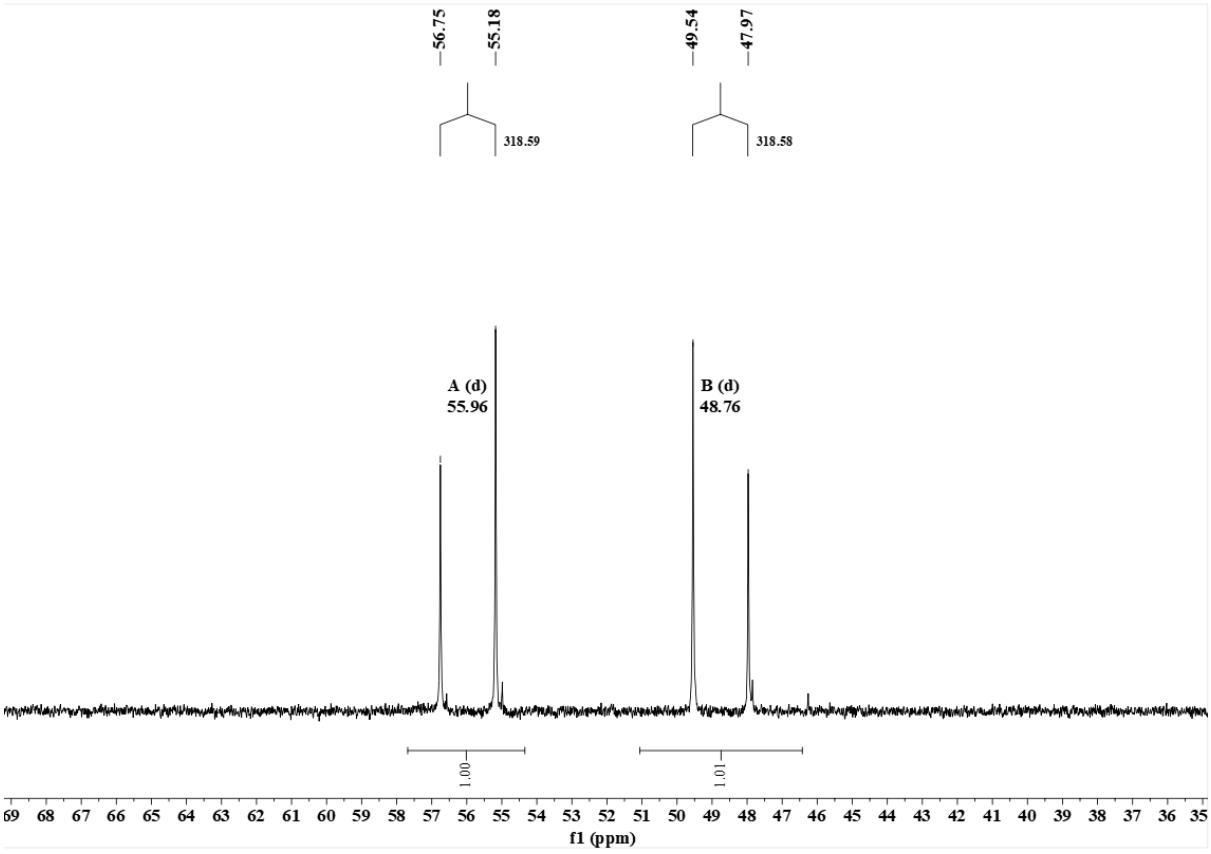

Figure S25- ^{31}P NMR spectrum of **[Pd-Br-Pd]**$^{+}$ (202 MHz, CD_2Cl_2, -60 °C).

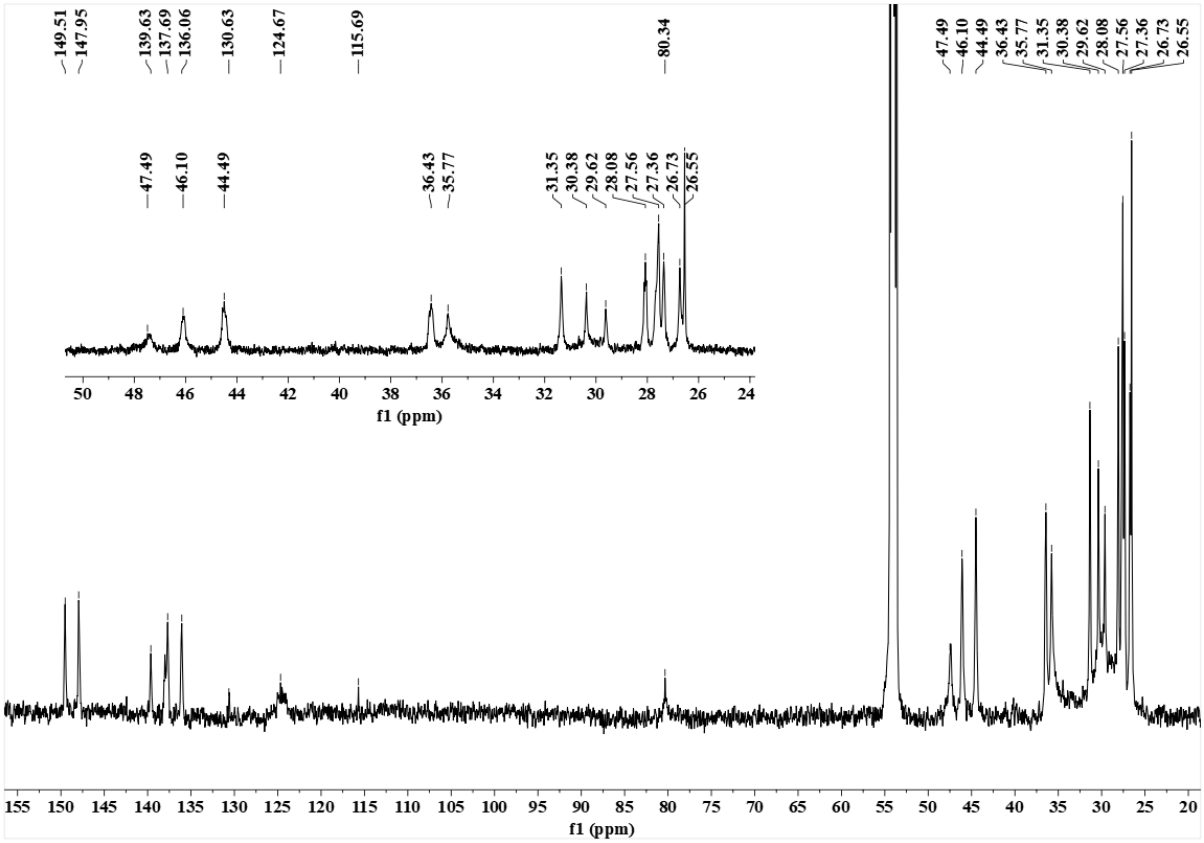

Figure S26- ^{13}C NMR spectrum of **[Pd-Br-Pd]**$^{+}$ (151 MHz, CD_2Cl_2, 25 °C). Signals at 130.63, 124.67 and 115.69 ppm are residual PhF.

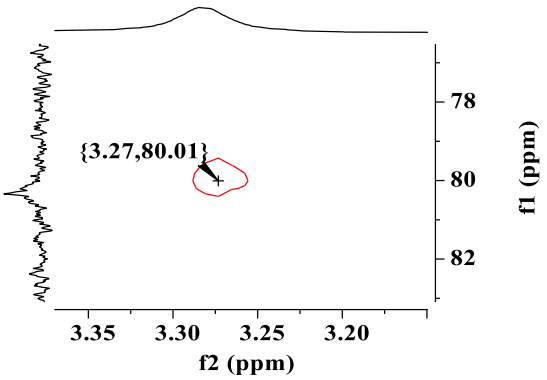

Figure S27- Section of ^{1}H-^{13}C HSQC NMR spectrum of **[Pd-Br-Pd]**$^{+}$ showing the Pd-CH cross peak (600, 151 MHz, CD_2Cl_2, 25 °C).

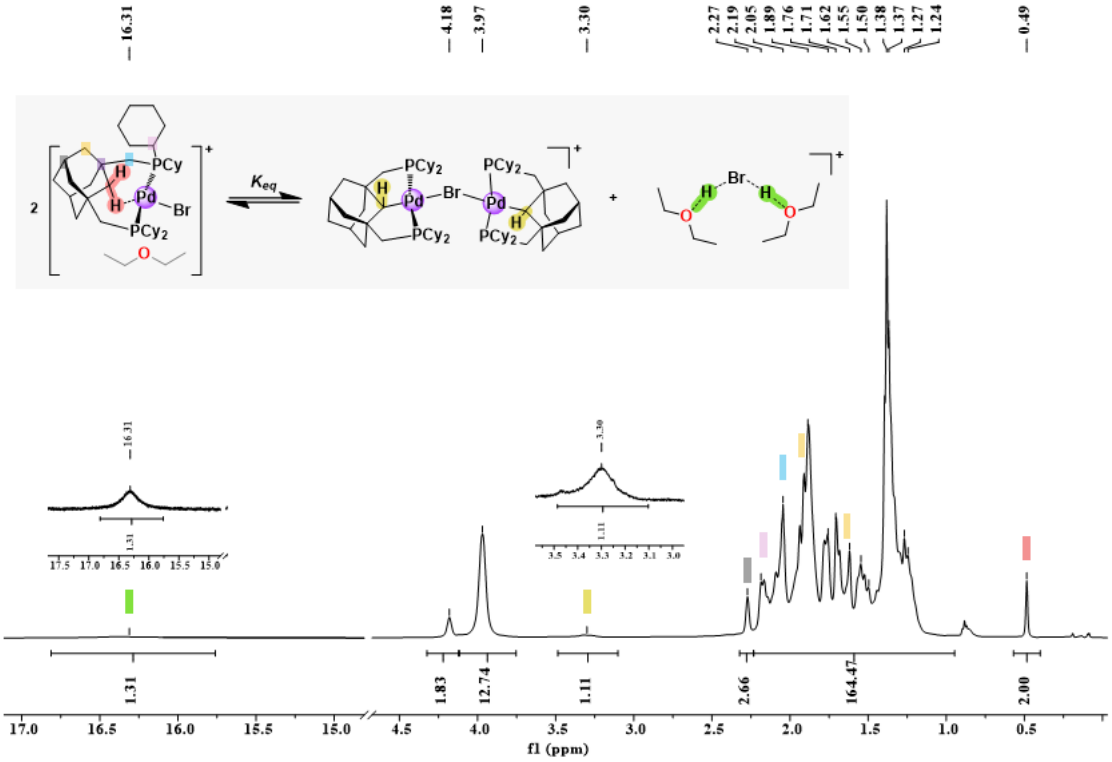

Figure S28- ^{1}H NMR spectrum of the equilibrium mixture after protonation of **[PdBr]** with $H(Et_2O)_2[B(C_6F_5)_4]$, showing a mixture of **[PdCH$_2$•Et$_2$O]**$^+$, **[Pd-Br-Pd]**$^+$, and **[HBrH•2OEt$_2$]**$^+$ (500 MHz, CD_2Cl_2, 25 °C).

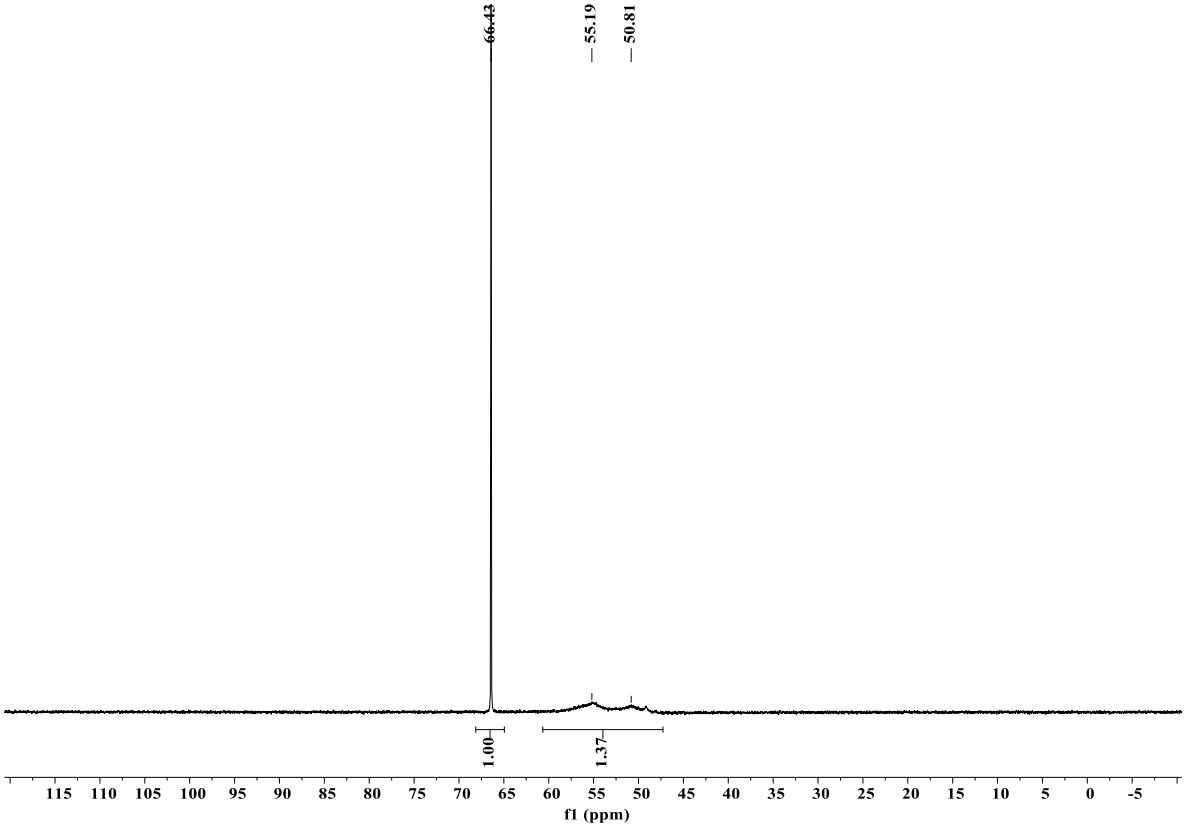

Figure S29- ^{31}P NMR spectrum of the equilibrium mixture after protonation of **[PdBr]** with $H(Et_2O)_2[B(C_6F_5)_4]$, showing a mixture of **[PdCH$_2$•Et$_2$O]**$^+$ and **[Pd-Br-Pd]**$^+$ (202 MHz, CD_2Cl_2, 25 °C).

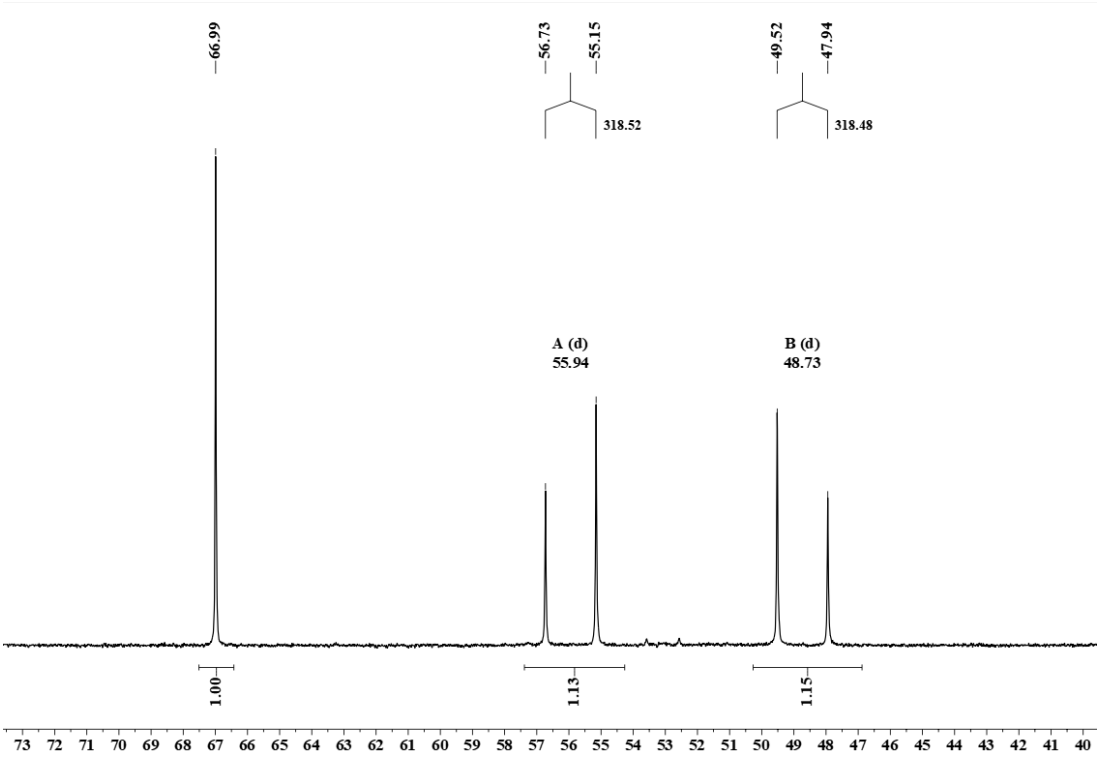

Figure S30- ^{31}P NMR spectrum of the equilibrium mixture after protonation of **[PdBr]** with $H(Et_2O)_2[B(C_6F_5)_4]$, showing a mixture of **[PdCH$_2$•Et$_2$O]**$^+$ and **[Pd-Br-Pd]**$^+$ (202 MHz, CD_2Cl_2, -60 °C).

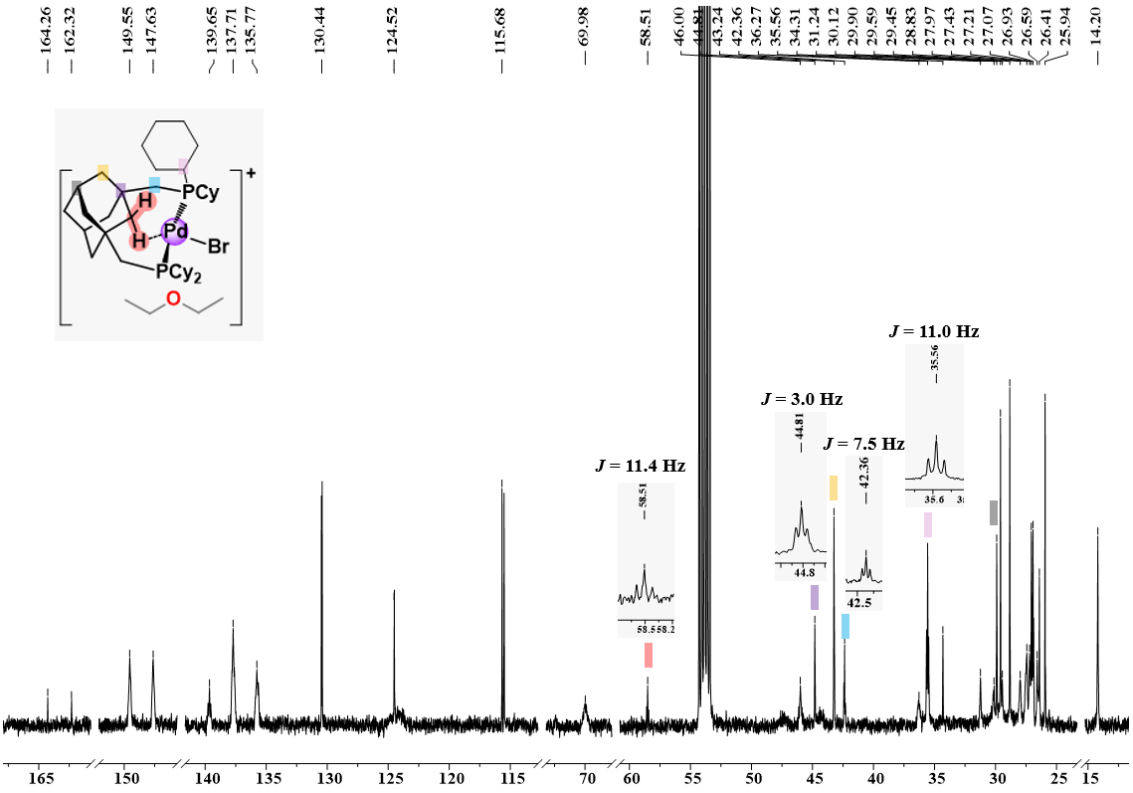

Figure S31- ^{13}C NMR spectrum of the equilibrium mixture after protonation of **[PdBr]** with $H(Et_2O)_2[B(C_6F_5)_4]$ (126 MHz, CD_2Cl_2, 25 °C). Signals at 130.44, 124.52 and 115.68 ppm are residual PhF.

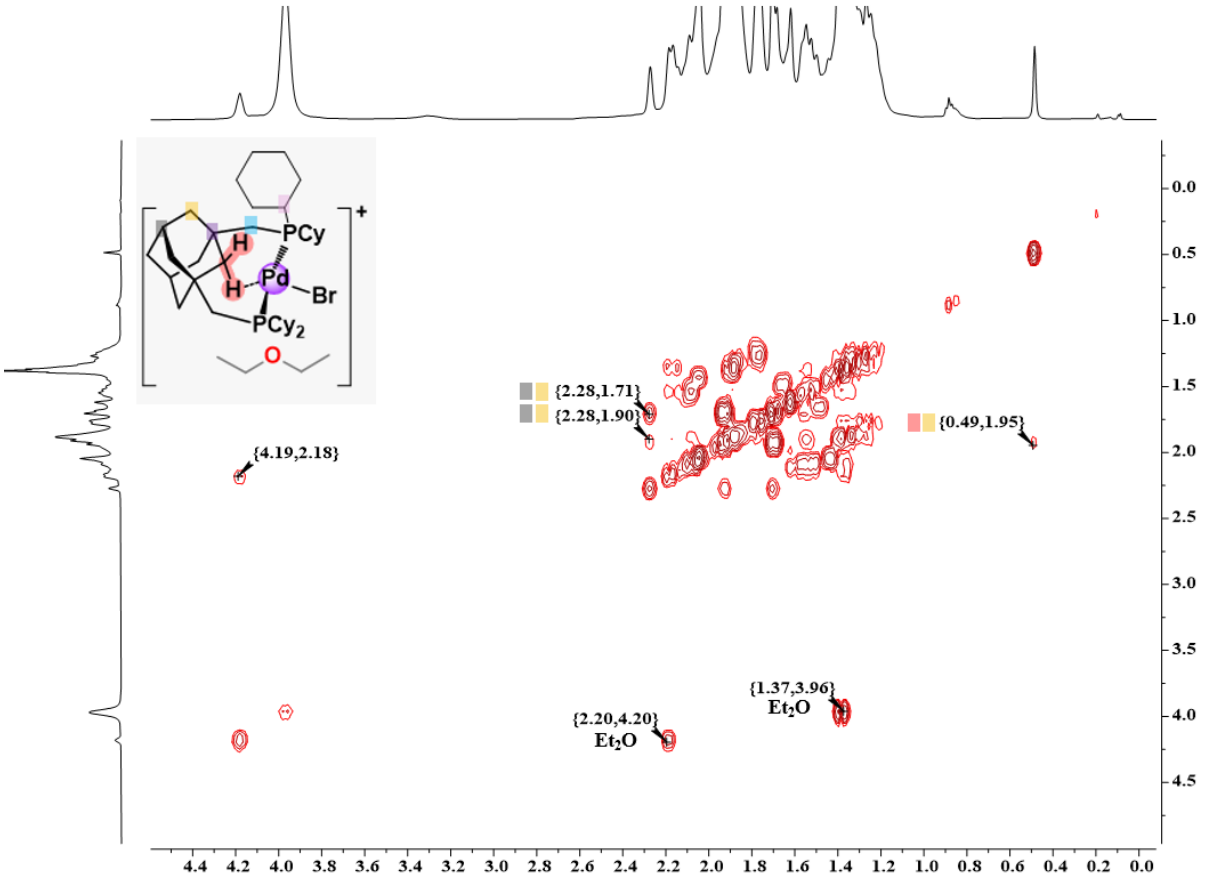

Figure S32- ^{1}H-^{1}H COSY NMR spectrum of the equilibrium mixture after protonation of **[PdBr]** with $H(Et_2O)_2[B(C_6F_5)_4]$ (500, 500 MHz, CD_2Cl_2, 25 °C).

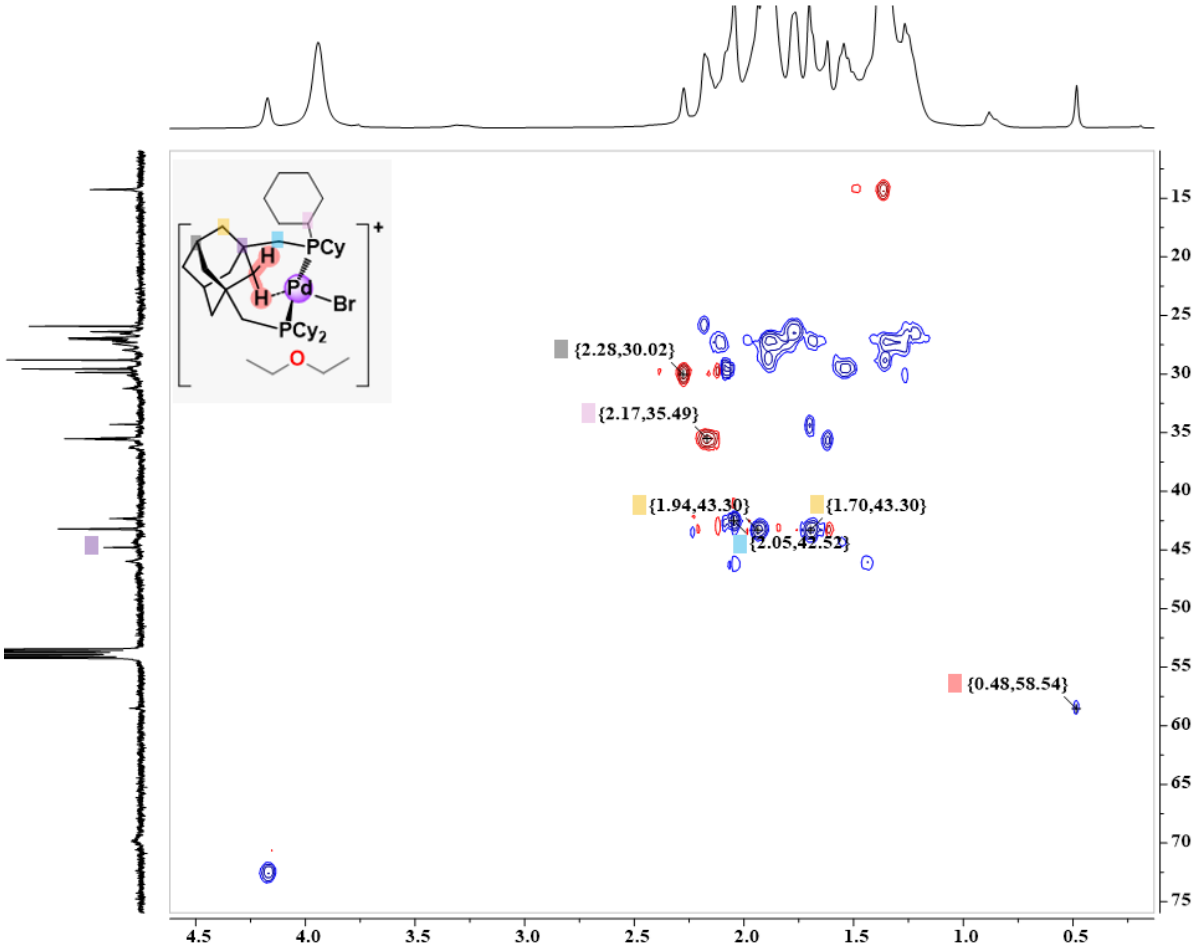

Figure S33- ^{1}H-^{13}C HSQC NMR spectrum of the equilibrium mixture after protonation of **[PdBr]** with $H(Et_2O)_2[B(C_6F_5)_4]$ (600, 151 MHz, CD_2Cl_2, 25 °C).

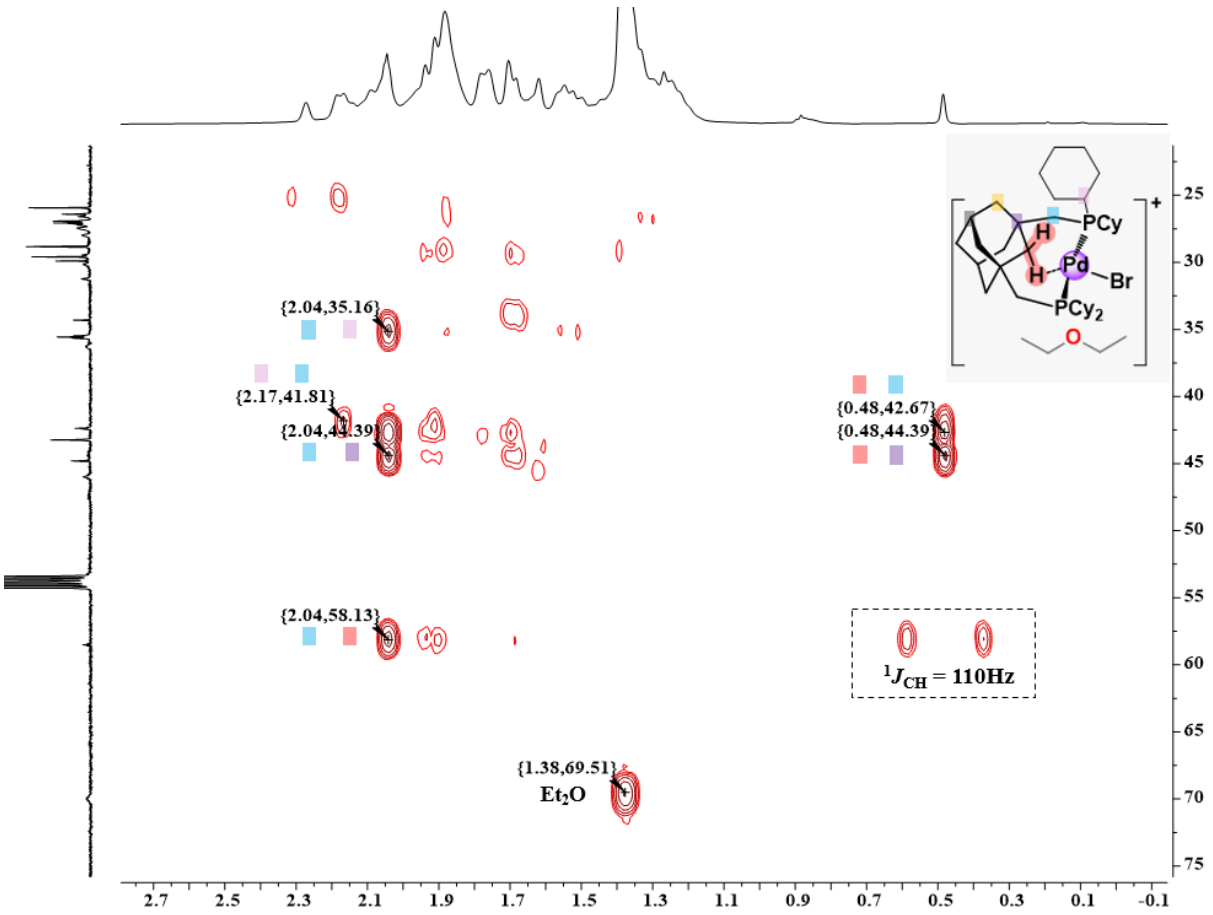

Figure S34- ^{1}H-^{13}C HMBC NMR spectrum of the equilibrium mixture after protonation of **[PdBr]** with $H(Et_2O)_2[B(C_6F_5)_4]$ (500, 126 MHz, CD_2Cl_2, 25 °C). Peaks in the dashed box are residual coupling from ^{1}H-^{13}C HSQC with $^{1}J_{CH}$ = 110 Hz

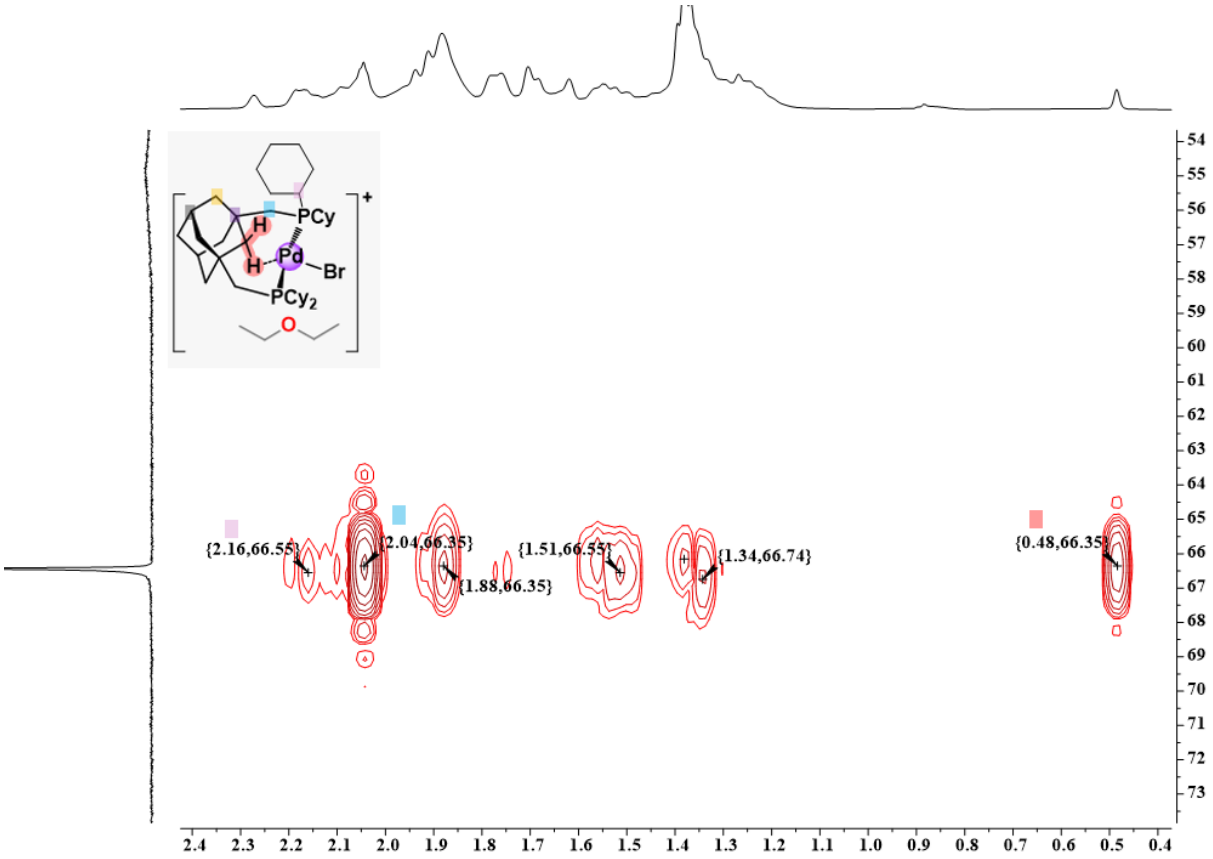

Figure S35- ^{1}H-^{31}P HMBC NMR spectrum of the equilibrium mixture after protonation of **[PdBr]** with $H(Et_2O)_2[B(C_6F_5)_4]$ (500, 202 MHz, CD_2Cl_2, 25 °C).

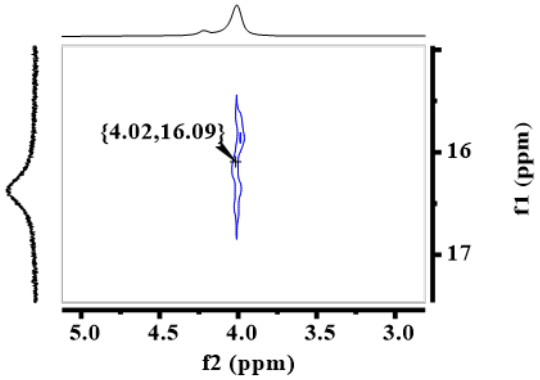

Figure S36- Section of ^{1}H-^{1}H NOESY (blue) NMR spectrum of the equilibrium mixture after protonation of **[PdBr]** with $H(Et_2O)_2[B(C_6F_5)_4]$ (500, 500 MHz, CD_2Cl_2, 25 °C, τ_m = 1.0 s, NS = 64), showing the Br*H*···OC*H*$_2$CH$_3$ cross peak from **[HBrH•2OEt$_2$]$^+$**.

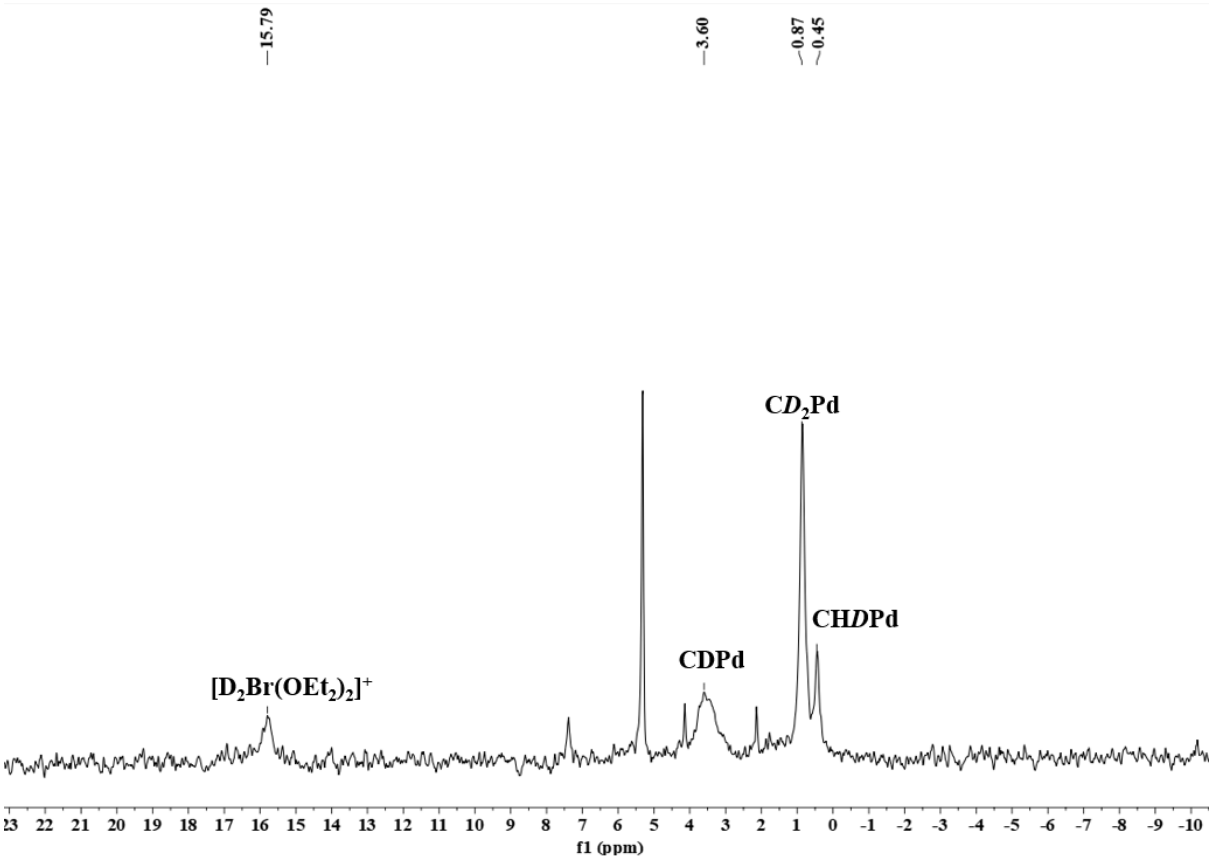

Figure S37- ^{2}H NMR spectrum of the equilibrium mixture after deuteration of **[PdBr]** with $D(Et_2O)_2[B(C_6F_5)_4]$ (77 MHz, CH_2Cl_2, 25 °C).

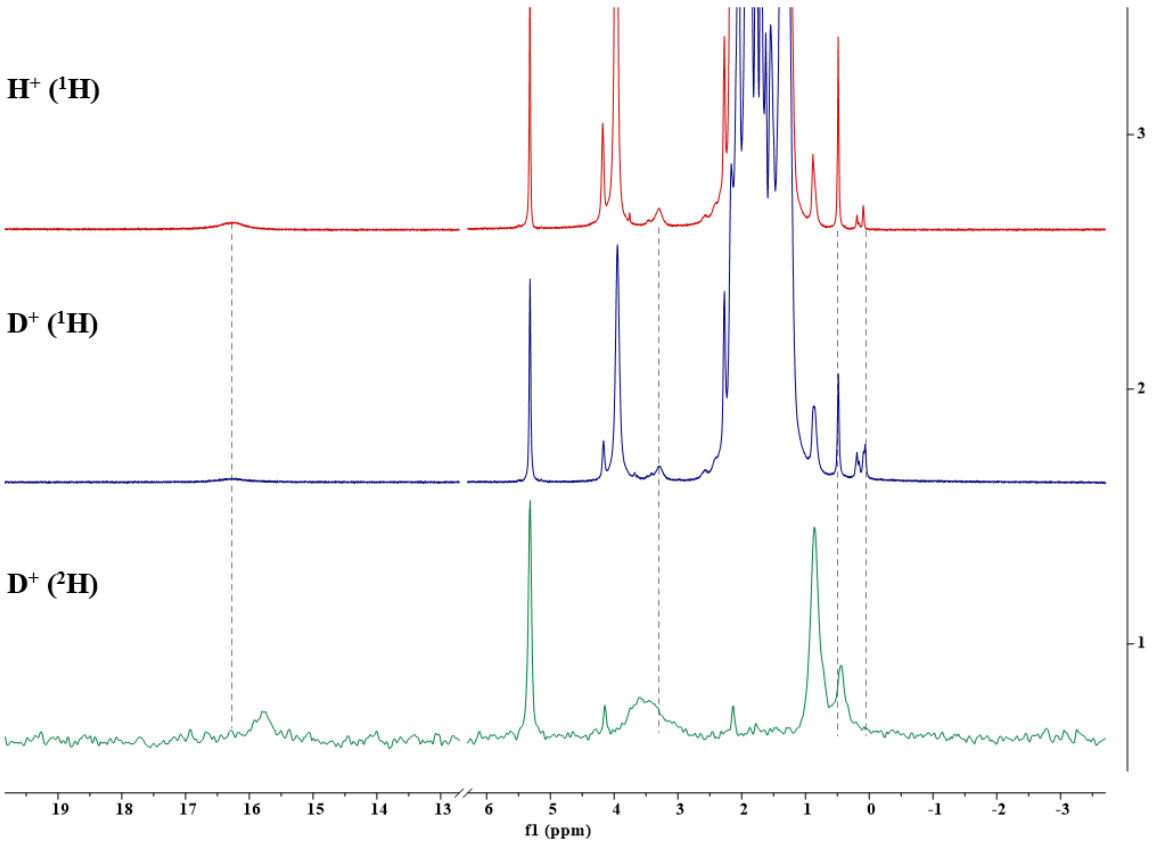

Figure S38- Comparison of ^{1}H NMR (top, red) spectrum of the equilibrium mixture after protonation of **[PdBr]** with $H(Et_2O)_2[B(C_6F_5)_4]$ (500MHz, CD_2Cl_2, 25 °C), ^{1}H NMR (middle, blue) spectrum of the equilibrium mixture after deuteration of **[PdBr]** with $D(Et_2O)_2[B(C_6F_5)_4]$ (500MHz, CD_2Cl_2, 25 °C) and ^{2}H NMR (bottom, green) spectrum of the equilibrium mixture after deuteration of **[PdBr]** with $D(Et_2O)_2[B(C_6F_5)_4]$ (500MHz, CH_2Cl_2, 25 °C).

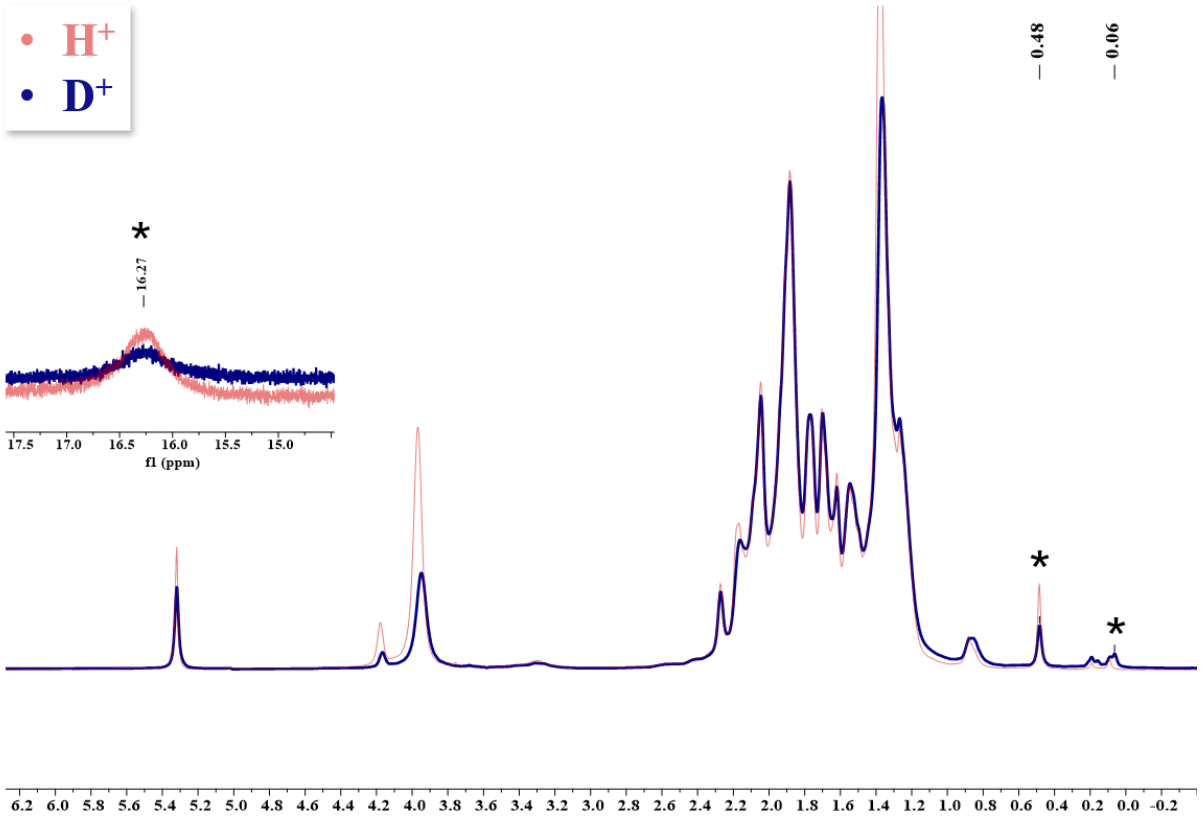

Figure S39- Comparison of ^{1}H NMR (red) spectrum of the equilibrium mixture after protonation of **[PdBr]** with $H(Et_2O)_2[B(C_6F_5)_4]$ (500MHz, CD_2Cl_2, 25 °C) and ^{1}H NMR (blue) spectrum of the equilibrium mixture after deuteration of **[PdBr]** with $D(Et_2O)_2[B(C_6F_5)_4]$ (500MHz, CD_2Cl_2, 25 °C). Peaks at 3.97 and 1.38 ppm are interacting Et_2O. The main differences between two spectrums are highlighted with asterisk.

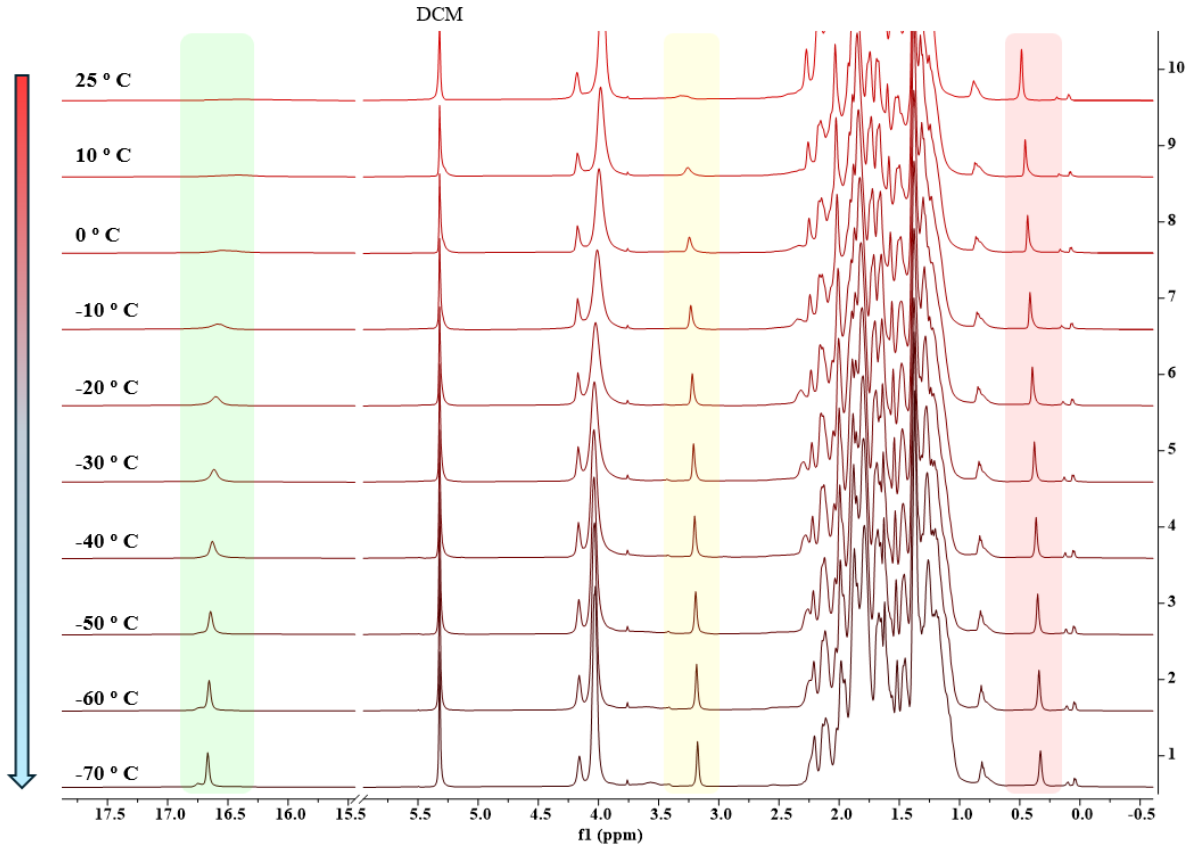

Figure S40- Variable temperature ^{1}H NMR spectrum of the equilibrium mixture after protonation of **[PdBr]** with $H(Et_2O)_2[B(C_6F_5)_4]$ (500 MHz, CD_2Cl_2).

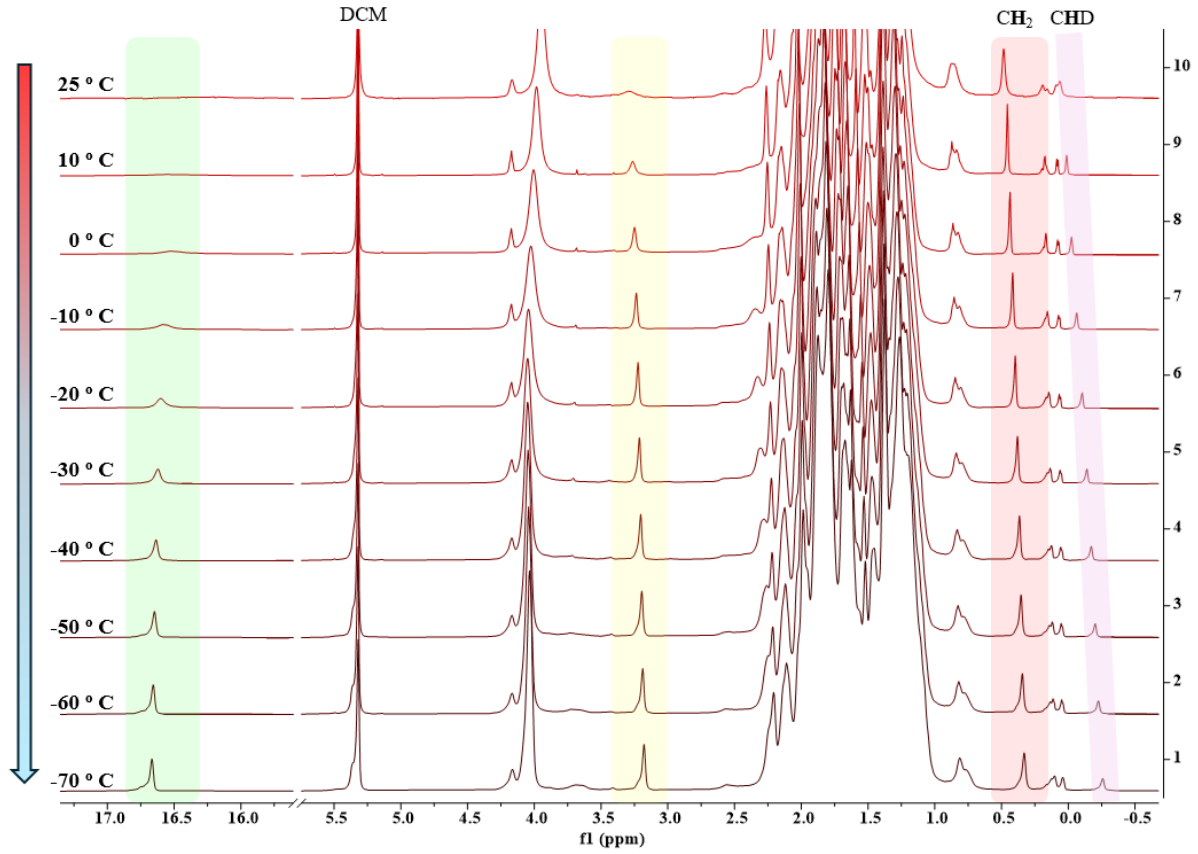

Figure S41- Variable temperature ^{1}H NMR spectrum of the equilibrium mixture after protonation of **[PdBr]** with $D(Et_2O)_2[B(C_6F_5)_4]$ (500 MHz, CD_2Cl_2).

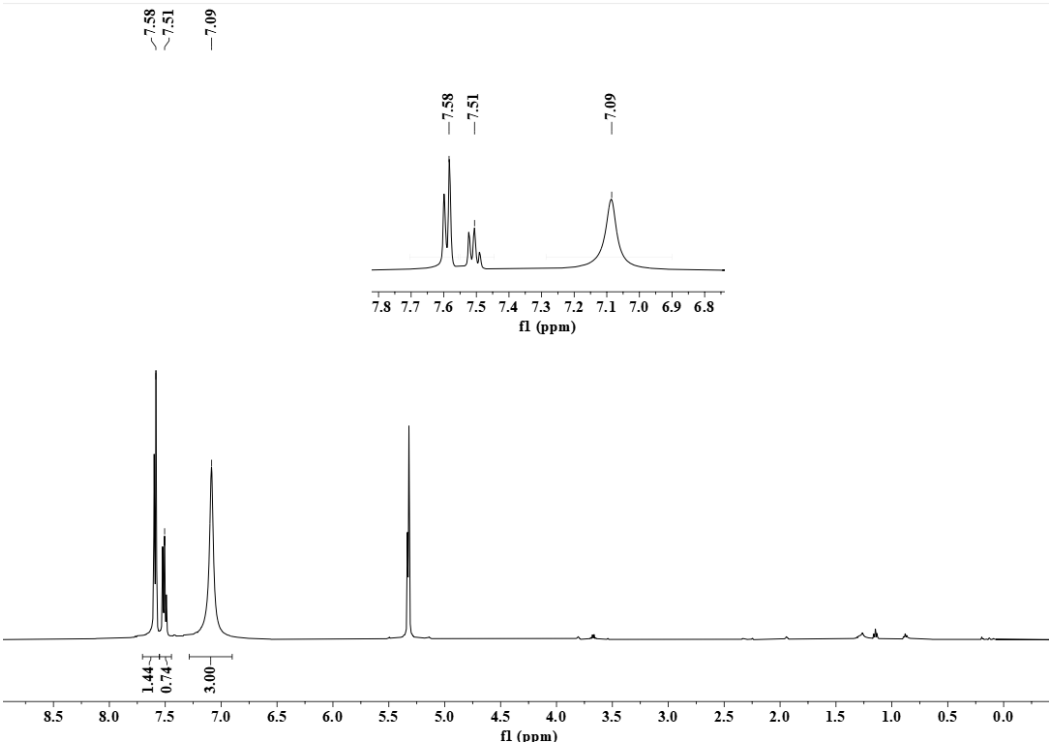

Figure S42- ^{1}H NMR spectrum of **[H_3NAr^{Cl}][$B(C_6F_5)_4$]** (500MHz, CD_2Cl_2, 25 °C). Signals at and 3.66, 1.26, 1.16 and 0.88 ppm are residual Et_2O and pentane in the NMR solvent.

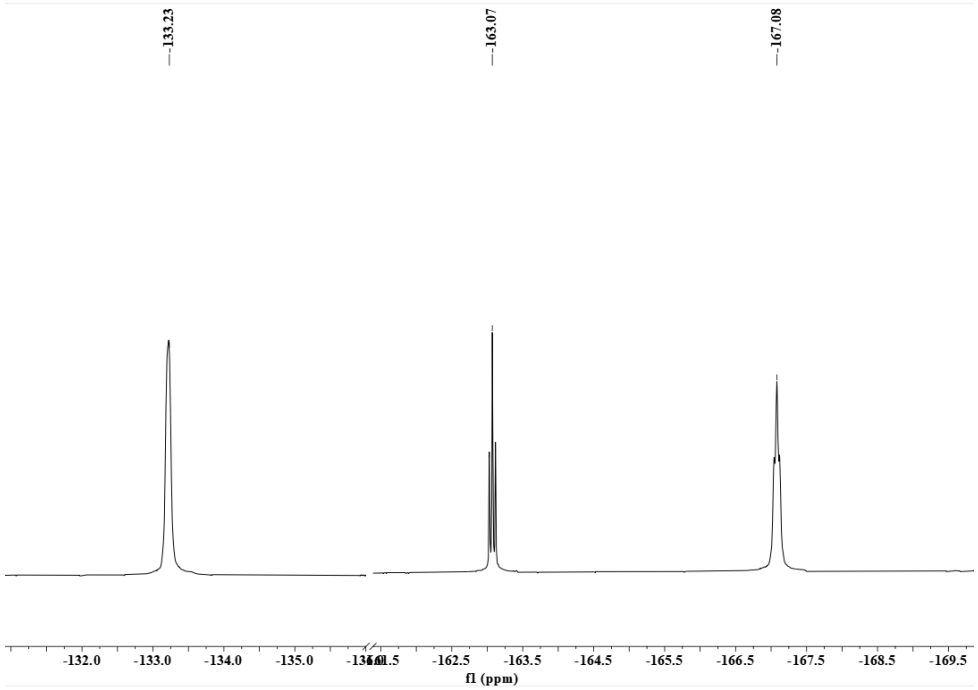

Figure S43- ^{19}F NMR spectrum of **[H_3NAr^{Cl}][$B(C_6F_5)_4$]** (471 MHz, CD_2Cl_2, 25 °C).

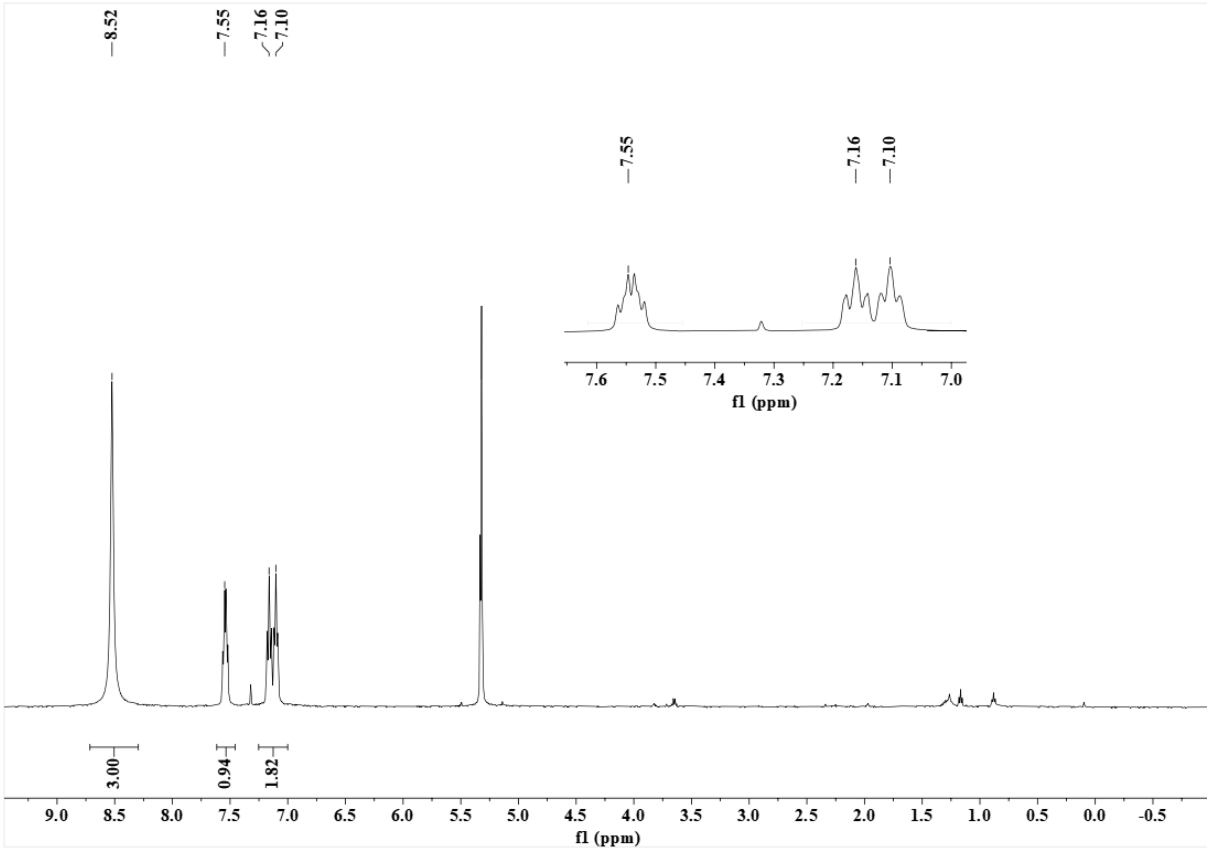

Figure S44- ^{1}H NMR spectrum of **[H_3NAr^{F}][$B(C_6F_5)_4$]** (500 MHz, CD_2Cl_2, 25 °C). Signal at 7.32ppm is impurity from NMR solvent. Signals at and 3.66, 1.26, 1.16 and 0.88 ppm are Et_2O and pentane in the NMR solvent.

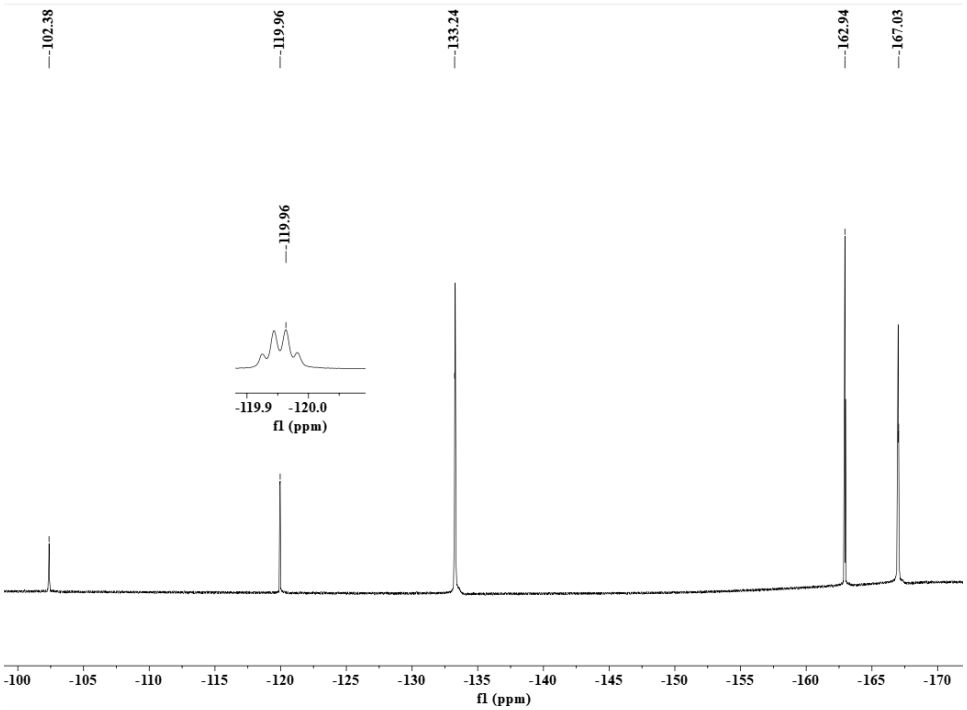

Figure S45- ^{19}F NMR spectrum of **[H_3NAr^F][$B(C_6F_5)_4$]** (471 MHz, CD_2Cl_2, 25 °C).

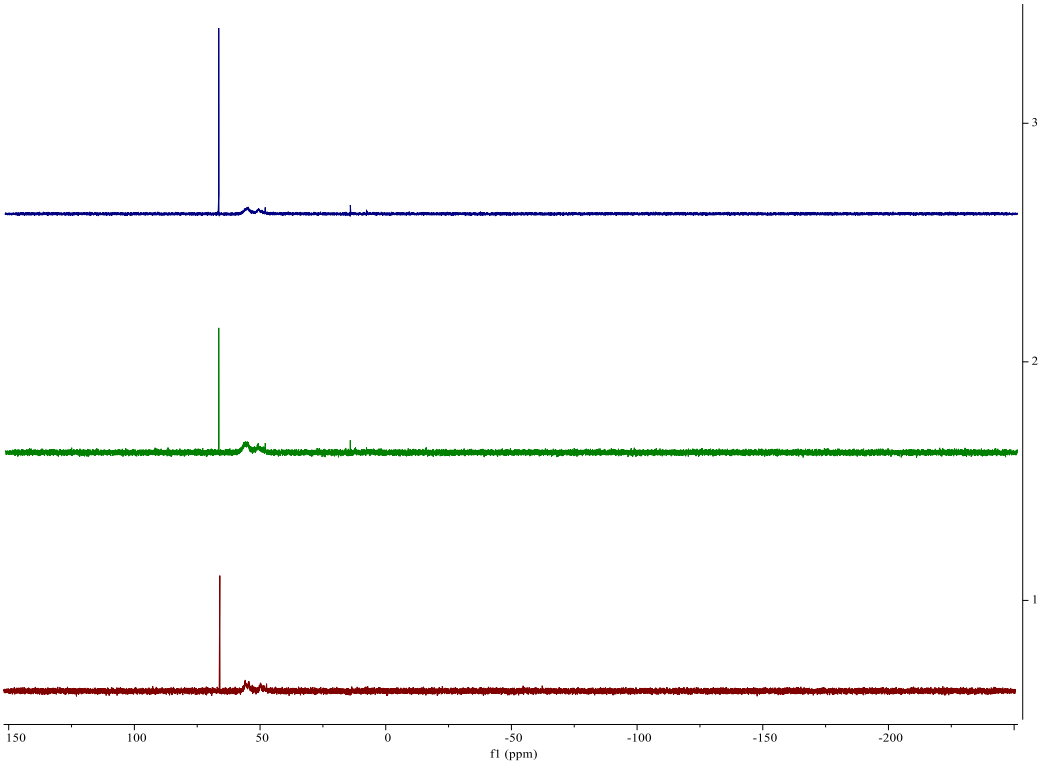

Figure S46- ^{31}P NMR spectrum of the reaction before (top, blue)) and after (middle, green) adding 2,4-dinitroaniline to the equilibrium mixture from protonation of **[PdBr]** with $H(Et_2O)_2[B(C_6F_5)_4]$ (202 MHz, CD_2Cl_2, 25 °C), and the ^{31}P NMR spectrum after drying and redissolving in DCE (bottom, red) (202 MHz, DCE with acetone-d_6 insert, 25 °C). No notable changes were observed in any spectra.

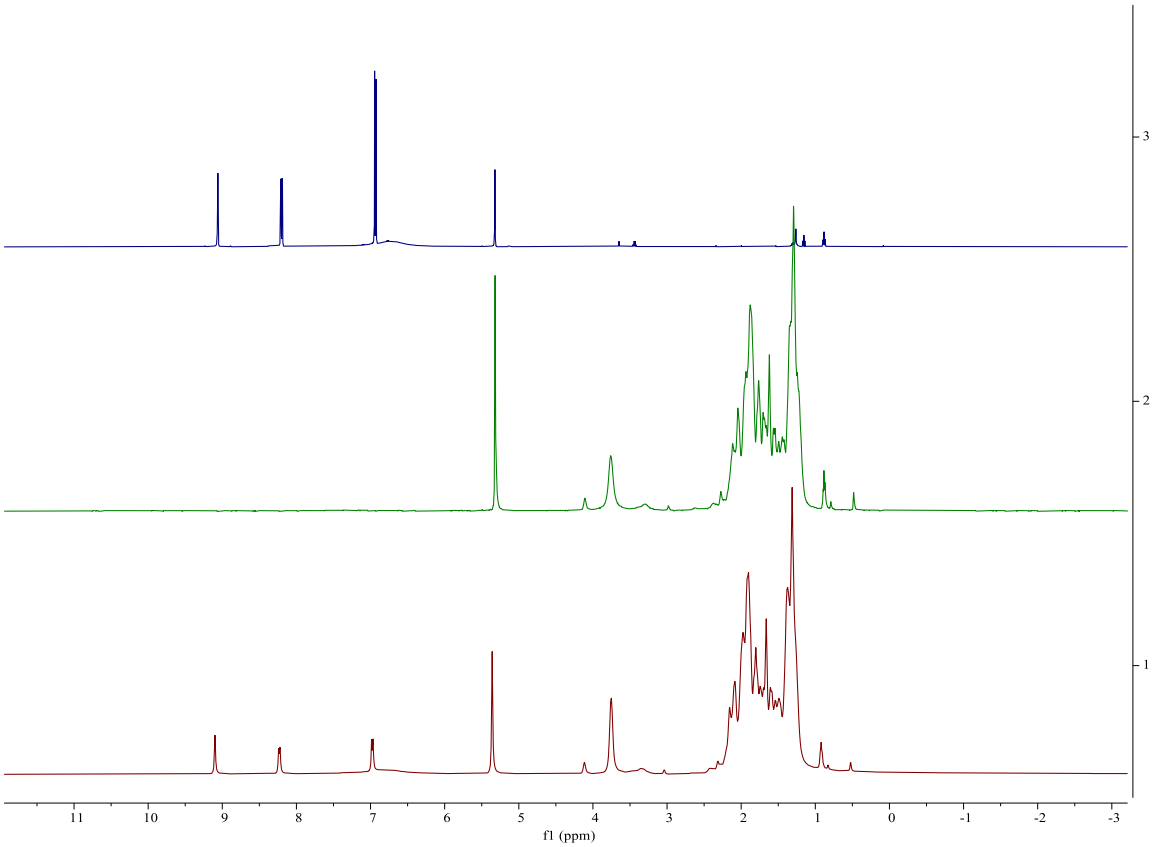

Figure S47- ^{1}H NMR spectrum of 2,4-dinitroaniline (top, blue), the reaction before (middle, green) and after (bottom, red) adding 2,4-dinitroaniline to the equilibrium mixture from protonation of **[PdBr]** with $H(Et_2O)_2[B(C_6F_5)_4]$ (500 MHz, CD_2Cl_2, 25 °C). No notable changes were observed in any spectra.

DOSY NMR and External Calibration Curve Analysis

We opted to use a DOSY NMR calibration curve method developed by Stalke.[12-14] The correlation between diffusion coefficient and molecular weight can be described by the following equation:

$$D = K \cdot MW_{det}^{\alpha} \tag{S16}$$

where D is diffusion coefficient, MW_{det} is the determined molecular weight, K and α are external calibration curve (ECC) fit parameters. Using the existing ECCs led to poor fits with the molecules in this study because the published ECCs do not contain heavy atoms such as Br and Pd, which have a disproportionate effect on molecular density.[13] Thus, it was necessary to construct a new heavy atom ECC using molecules of comparable molar densities and geometries. This was achieved by measuring D in CD_2Cl_2 and using $\log D_{ref,fix}$ = -8.5190 with the merged curve data (ECC_{Merge}^{CD2Cl2}) where $\log K$ = -7.55 and α = -0.535.[14] The following equations were used to create the calibration curves:[14]

$$logD_{x,norm} = logD_{ref,fix} - logD_{ref} + logD_x \tag{S17}$$

$$MW_{det} = 10^{\left(\frac{log_{Dx,norm} - logK}{\alpha}\right)} \tag{S18}$$

In equation S17, D_{ref} is the diffusion coefficient for solvent (CH_2Cl_2), D_x is the diffusion coefficient for the analyte, and $D_{x,norm}$ is the normalized diffusion coefficient. The following six molecules were used to construct the ECC: 1,3-bis(bromomethyl)adamantane (**AdBr**), 1,3-bis(dicyclohexylphosphino)adamantane (**AdPCy$_2$**), **[H$_3$NAr^F][B(C$_6$F$_5$)$_4$]**, **[H$_3$NAr^{Cl}][B(C$_6$F$_5$)$_4$]**, **[PdBr]**, and **[Pd-Br-Pd][B(C$_6$F$_5$)$_4$]**. The determined molecular weights (MW_{det}) were plotted against the actual molecular weight (MW_{act}) and used to construct a new ECC (Table S13 and Figure S48). See the Experimental section for spectrometer information, DOSY NMR experimental parameters, and sample preparation details.

Table S13- Analyte diffusion coefficients (D_x) and determined molecular weight (MW_{det}) for the molecules used in the heavy atom ECC.

	D_{ref} ($m^2/s\times10^{-9}$)	D_x ($m^2/s\times10^{-9}$)	log(D_{ref})	log(D_x)	log($D_{x,norm}$)	MW_{det} (g/mol)	MW_{act} (g/mol)
[H$_3$NAr^F]$^+$	3.26 ± 0.16	1.87 ± 0.21	-8.48	-8.73	-8.76	183 ± 21	130
[H$_3$NAr^{Cl}]$^+$	3.03 ± 0.03	1.55 ± 0.08	-8.52	-8.81	-8.81	226 ± 12	163
AdBr	3.68 ± 0.25	1.33 ± 0.05	-8.43	-8.88	-8.96	435 ± 16	322
AdPCy$_2$	3.56 ± 0.34	1.09 ± 0.08	-8.45	-8.96	-9.03	590 ± 43	557
[PdBr]	3.77 ± 0.42	0.81 ± 0.13	-8.42	-9.09	-9.19	1143 ± 183	741
[Pd-Br-Pd]$^+$	3.98 ± 0.14	0.69 ± 0.05	-8.40	-9.16	-9.28	1691 ± 123	1403

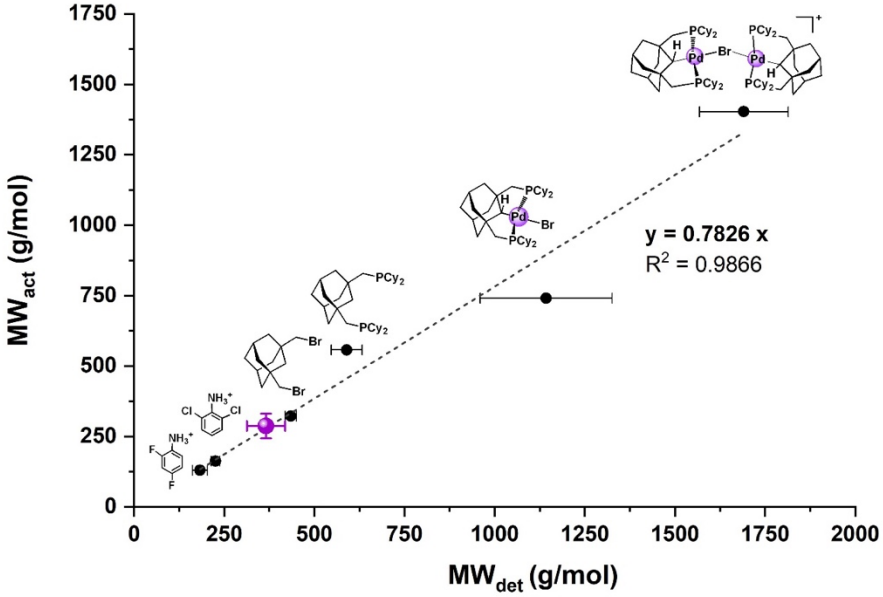

Figure S48- Heavy atom DOSY calibration curve using ECC data from Table S13. Based on its diffusion coefficient data, the corrected molecular weight (MW_{corr}) of the putative **[H$_2$Br(H$_3$NAr^F)$_2$]$^+$** is shown on the calibration curve in purple.

From the above calibration curve, it is seen that $MW_{act} = 0.7826 \bullet MW_{det}$ which is then used to determine the calculated solution-phase molecular weight (MW_{cal}) of the adduct containing $\mathbf{[H_3NAr^F]^+}$ participating in equilibrium K_2 (see main text). Two molecules of the anilinium cation are proposed to aggregate with bromide to generate the cation $\mathbf{[H_2Br(H_3NAr^F)_2]^+}$ with a molecular weight of 340 g/mol. To test this hypothesis, two independently prepared equilibrium mixtures K_2 were prepared in CD_2Cl_2 and diffusion coefficients D_x were measured for the aromatic C-H resonances at 7.23 ppm and 7.65 ppm (Table S14). As a result, MW_{cal} = 287 ± 44 g/mol, which matches well with the molecular weight of $\mathbf{[H_2Br(H_3NAr^F)_2]^+}$ (340 g/mol).

Table S14- Analyte diffusion coefficient and molecular weight data for the aromatic resonances of two independently prepared samples containing the 2,4-difluoroanilinium cation (D_x) in equilibrium K_2 in CD_2Cl_2.

δ (ppm)	D_{ref} ($m^2/s \times 10^{-9}$)	D_x ($m^2/s \times 10^{-9}$)	log(D_{ref})	log(D_x)	log($D_{x,norm}$)	MW_{det} (g/mol)	MW_{cal} (g/mol)
7.23	132.9 ± 5.6	52.57 ± 5.49	-6.88	-7.28	-8.92	367	287
7.65	132.9 ± 5.6	55.30 ± 9.80	-6.88	-7.26	-8.90	333	261
7.23	1.88 ± 0.05	0.67 ± 0.07	-8.73	-9.18	-8.97	445	348
7.65	3.01 ± 0.08	1.28 ± 0.11	-8.52	-8.89	-8.89	320	250
					Average:	366 ± 53	**287 ± 44**

Electrochemistry

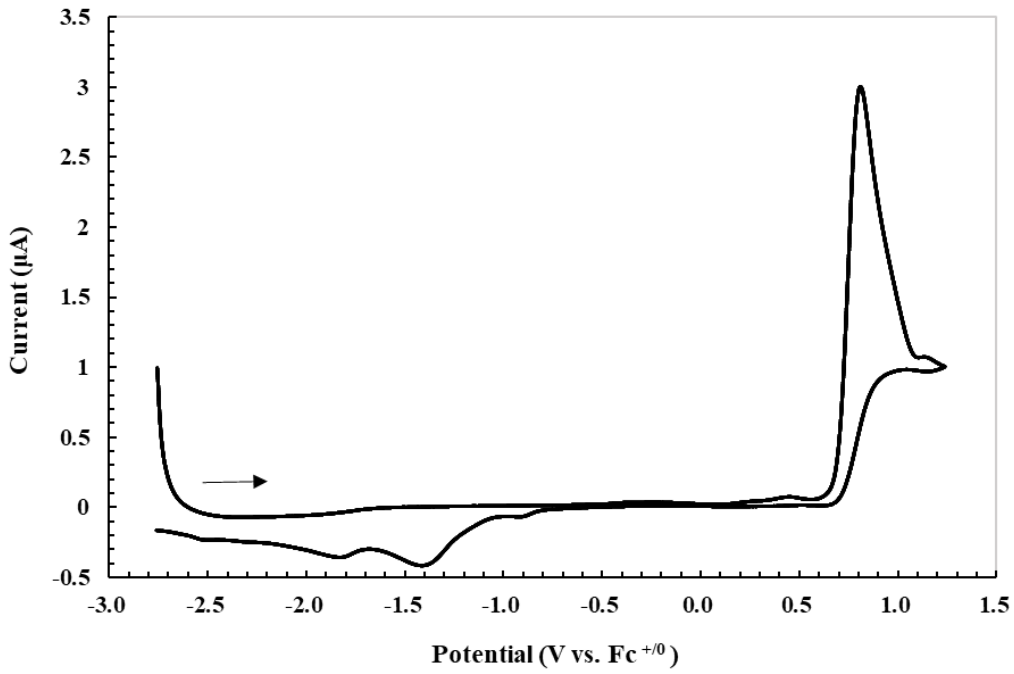

Figure S49- Cyclic voltammograms of **[PdBr]** in THF after background subtraction. Conditions: 1 mM analyte, 0.2 M $[^nBu_4N][B(C_6F_5)_4]$, scan rate 100 mV/s.

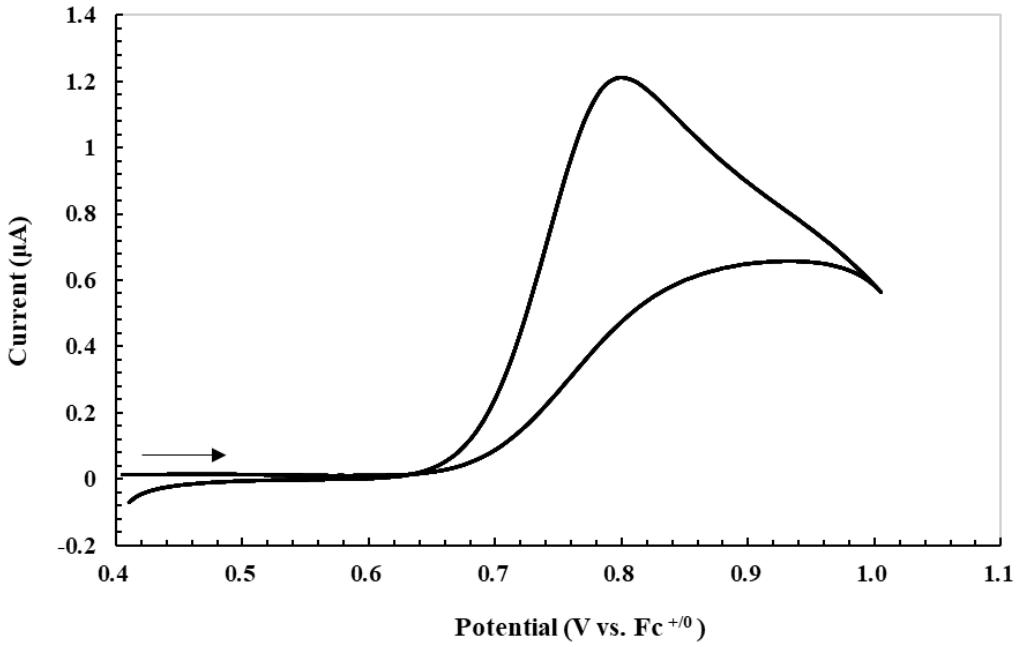

Figure S50- Cyclic voltammograms of **[PdBr]** in THF after background subtraction. Conditions: 1 mM analyte, 0.2 M [^{n}Bu$_4$N][B(C$_6$F$_5$)$_4$], scan rate 100 mV/s. E_{pa} = 0.810 V vs. Fc$^{+/0}$.

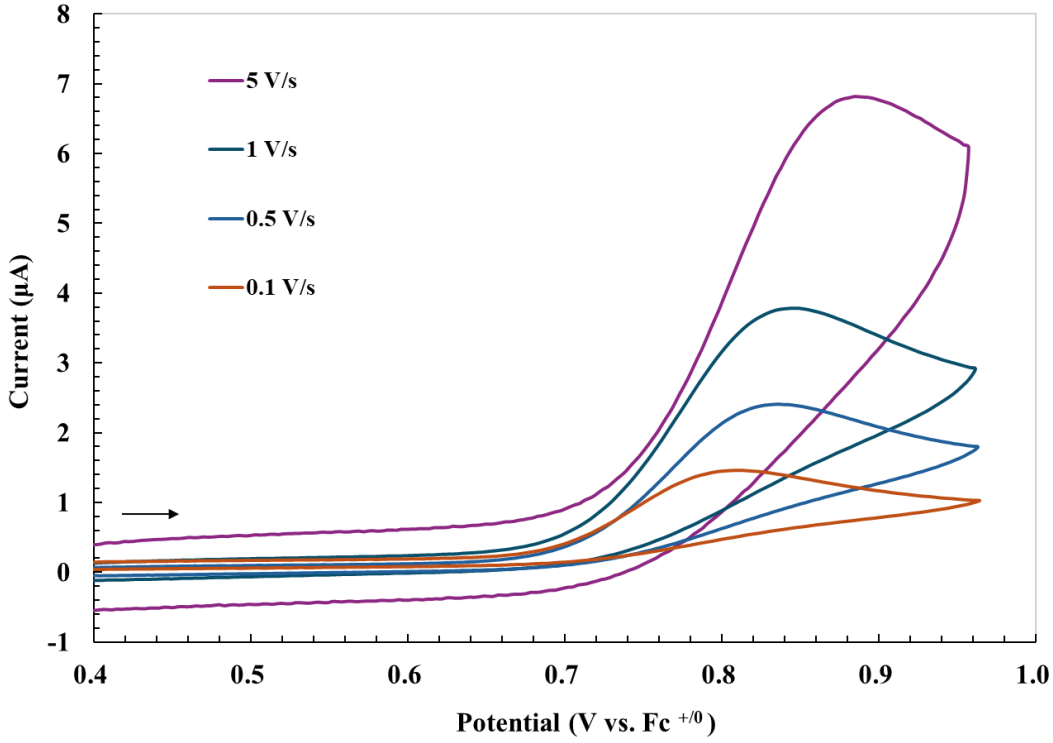

Figure S51- Cyclic voltammograms of **[PdBr]** in THF at different scan rates. Conditions: 1 mM analyte, 0.2 M [^{n}Bu$_4$N][B(C$_6$F$_5$)$_4$].

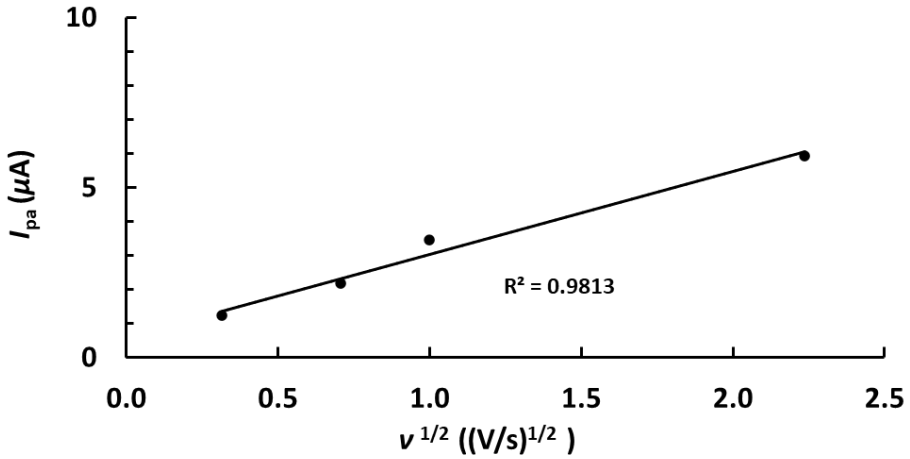

Figure S52- Anodic peak current (I_{pa}) *vs.* the square root of scan rate $v^{1/2}$ of **[PdBr]** in THF. Conditions: 1 mM analyte, 0.2 M [^{n}Bu$_4$N][B(C$_6$F$_5$)$_4$].

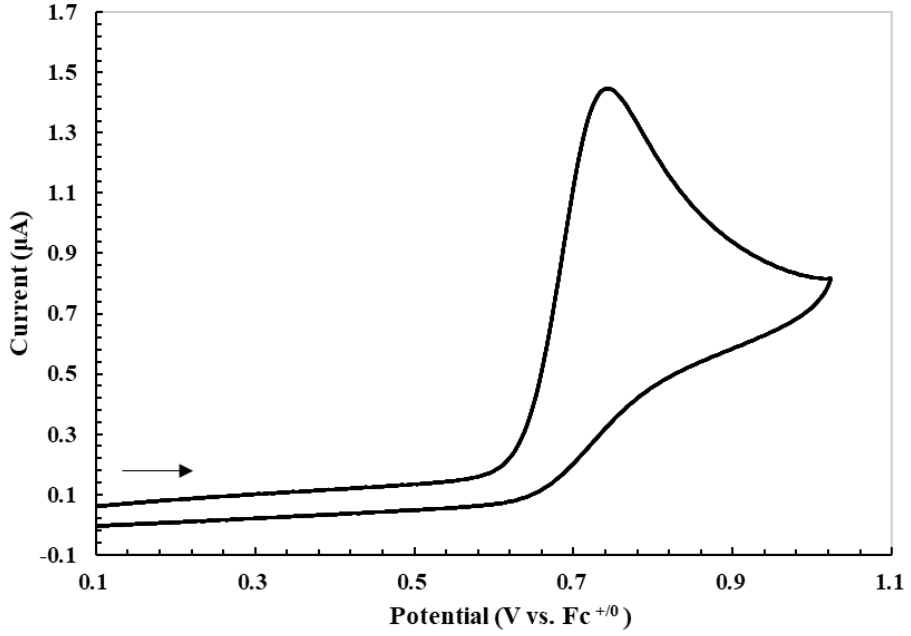

Figure S53- Cyclic voltammograms of **[PdBr]** in PhF. Conditions: 1 mM analyte, 0.2 M [^{n}Bu$_4$N][B(C$_6$F$_5$)$_4$], scan rate 100 mV/s. E_{pa} = 0.762 V vs. Fc$^{+/0}$.

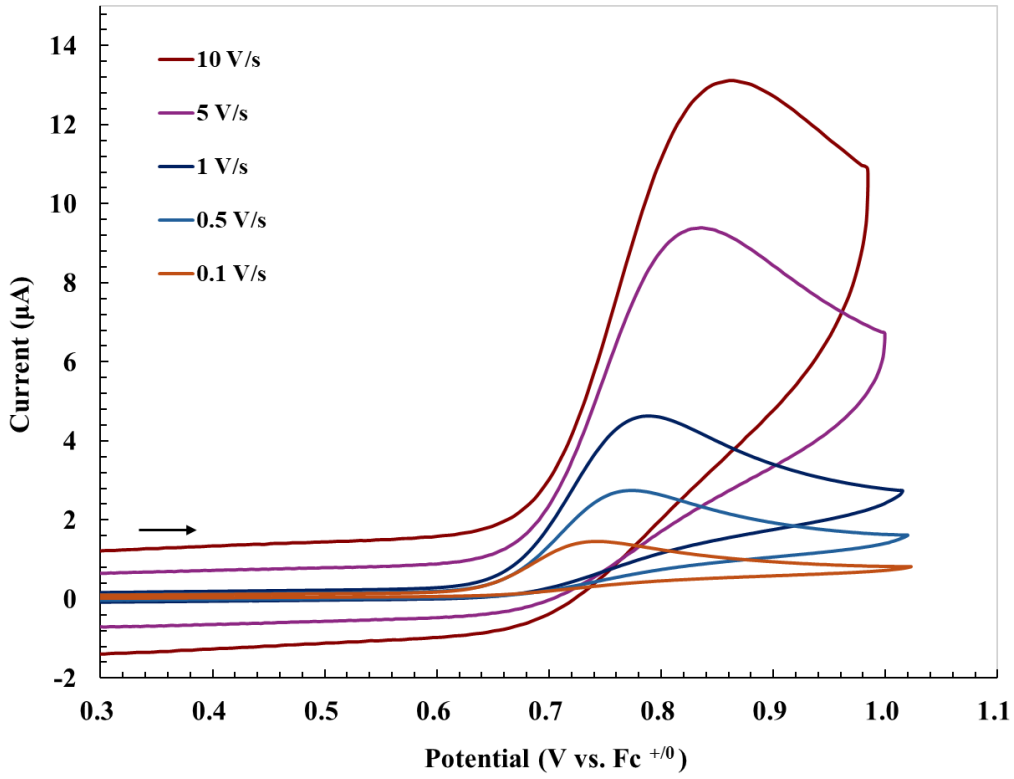

Figure S54- Cyclic voltammograms of **[PdBr]** in PhF at different scan rates. Conditions: 1 mM analyte, 0.2 M [^{n}Bu$_4$N][B(C$_6$F$_5$)$_4$].

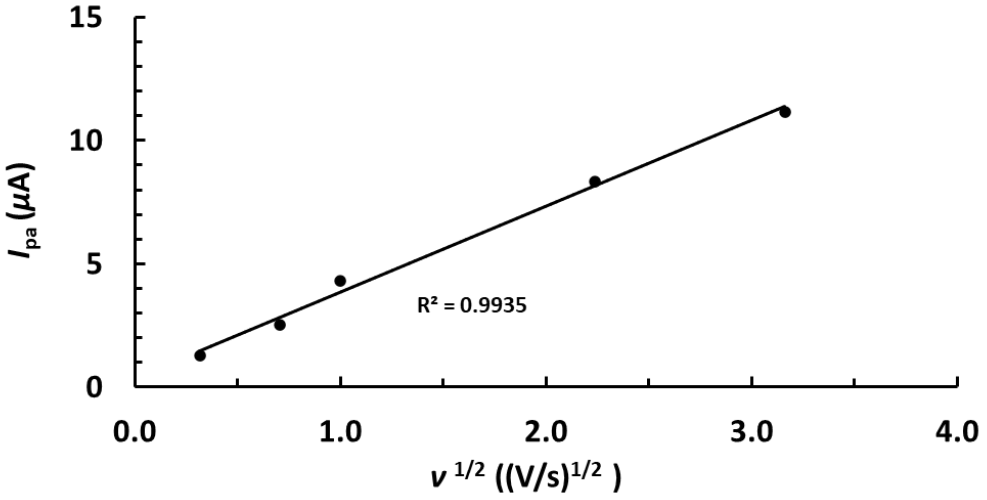

Figure S55- Anodic peak current (I_{pa}) *vs.* the square root of scan rate $v^{1/2}$ of **[PdBr]** in PhF. Conditions: 1 mM analyte, 0.2 M [^{n}Bu$_4$N][B(C$_6$F$_5$)$_4$].

References

(1) Williams, D. B. G.; Lawton, M. Drying of Organic Solvents: Quantitative Evaluation of the Efficiency of Several Desiccants. *J. Org. Chem.* **2010**, *75* (24), 8351-8354.

(2) Averina, E. B.; Sedenkova, K. N.; Bakhtin, S. G.; Grishin, Y. K.; Kutateladze, A. G.; Roznyatovsky, V. A.; Rybakov, V. B.; Butov, G. M.; Kuznetsova, T. S.; Zefirov, N. S. symm-Tetramethylenecyclooctane: en route to polyspirocycles. *J Org Chem* **2014**, *79* (17), 8163-8170.

(3) Gerber, R.; Blacque, O.; Frech, C. M. Suzuki Cross-Coupling Reactions Catalyzed by an Aliphatic Phosphine-Based Pincer Complex of Palladium: Evidence for a Molecular Mechanism. *ChemCatChem* **2009**, *1* (3), 393-400.
(4) Heiden, Z. M.; Chen, S.; Mock, M. T.; Dougherty, W. G.; Kassel, W. S.; Rousseau, R.; Bullock, R. M. Protonation of Ferrous Dinitrogen Complexes Containing a Diphosphine Ligand with a Pendent Amine. *Inorg. Chem.* **2013**, *52* (7), 4026-4039.
(5) LeSuer, R. J.; Geiger, W. E. Improved Electrochemistry in Low-Polarity Media Using Tetrakis(pentafluorophenyl)borate Salts as Supporting Electrolytes. *Angew. Chem. Int. Ed.* **2000**, *39* (1), 248-250.
(6) Fulmer, G. R.; Miller, A. J. M.; Sherden, N. H.; Gottlieb, H. E.; Nudelman, A.; Stoltz, B. M.; Bercaw, J. E.; Goldberg, K. I. NMR Chemical Shifts of Trace Impurities: Common Laboratory Solvents, Organics, and Gases in Deuterated Solvents Relevant to the Organometallic Chemist. *Organometallics* **2010**, *29* (9), 2176-2179.
(7) Castañar, L.; Poggetto, G. D.; Colbourne, A. A.; Morris, G. A.; Nilsson, M. The GNAT: A new tool for processing NMR data. *Magnetic Resonance in Chemistry* **2018**, *56* (6), 546-558.
(8) Zimmer, K. D.; Shoemaker, R.; Ruminski, R. R. Synthesis and characterization of a fluxional Re(I) carbonyl complex fac-[Re(CO)3(dpop′)Cl] with the nominally tri-dentate ligand dipyrido(2,3-a:3′,2′-j)phenazine (dpop′). *Inorganica Chimica Acta* **2006**, *359* (5), 1478-1484.
(9) Spek, A. L. Structure validation in chemical crystallography. *Acta Crystallogr., Sect. D* **2009**, *65* (2), 148-155.
(10) Tshepelevitsh, S.; Kütt, A.; Lõkov, M.; Kaljurand, I.; Saame, J.; Heering, A.; Plieger, P. G.; Vianello, R.; Leito, I. On the Basicity of Organic Bases in Different Media. *Eur. J. Org. Chem.* **2019**, *2019* (40), 6735-6748.
(11) Kaupmees, K.; Järviste, R.; Leito, I. Basicity of Very Weak Bases in 1,2-Dichloroethane. *Chem. Eur. J.* **2016**, *22* (48), 17445-17449.
(12) Neufeld, R.; John, M.; Stalke, D. The Donor-Base-Free Aggregation of Lithium Diisopropyl Amide in Hydrocarbons Revealed by a DOSY Method. *Angew. Chem. Int. Ed.* **2015**, *54* (24), 6994-6998.
(13) Neufeld, R.; Stalke, D. Accurate molecular weight determination of small molecules via DOSY-NMR by using external calibration curves with normalized diffusion coefficients. *Chem. Sci.* **2015**, *6*, 3354-3364.
(14) Bachmann, S.; Neufeld, R.; Dzemski, M.; Stalke, D. New External Calibration Curves (ECCs) for the Estimation of Molecular Weights in Various Common NMR Solvents. *Chem. Eur. J.* **2016**, *22* (25), 8462-8465.